



An Integrated Approach to Unravel the Structural Controls on Groundwater Potentialities in Hyper-arid Regions Using Satellite and Land-Based Geophysics: A Case Study in Southwestern Desert of Egypt

Amin Ibrahim¹ · Khaled S. Gemal^{2,5}  · Sayed Bedair³ · Saada A. Saada⁴ · Magaly Koch⁵ · Ahmed Nosair²

Received: 15 November 2021 / Accepted: 28 November 2022 / Published online: 19 December 2022
© The Author(s), under exclusive licence to Springer Nature B.V. 2022

Abstract

Groundwater exploration is the most promising way to overcome water scarcity in hyper-arid regions around the world. Due to the scarcity of hydrogeological information in these regions, groundwater exploration is a challenging issue requiring the joint application of satellite and land-based information to delineate the groundwater aquifers in such harsh environments. In this research, an integrative approach was undertaken for groundwater exploration in the southwestern corner of Egypt as one of the most hyper-arid regions in North Africa. To fill the knowledge gap in this large area, two high-resolution satellite gravity datasets (EIGEN-6C4 and TOPEX-1min) were employed in combination with land-based geophysical surveys for a better understanding of groundwater potentialities in terms of structural controls. Further, the approaches of high-pass filter, tilt angle derivative, and enhanced horizontal gradient amplitude were used to analyze EIGEN-6C4 dataset. Additionally, 2D and 3D models along with a high-pass filtered gravity map were constructed to provide the subsurface barriers and preferential groundwater flow pathways. Several NNE windows have been recognized, particularly to the east of Gabel Kamel along Uweinat-Aswan uplifting allowing groundwater flow along northeastern structural trends. To verify this assumption, land-based magnetic and DC resistivity sounding surveys were executed at two selected sites based on the interpretation of satellite gravity and remote sensing data. The resistivity and 2D magnetic modeling reveal the presence of remarkable sub-basins with sufficient saturated sedimentary cover. Ultimately, the review of the different datasets, including satellite gravity and land-based geophysical investigations, facilitated the geological interpretation for detecting the structural controls on the groundwater flow paths and produced satisfactory results at shorter time frames and lower costs compared to typical groundwater exploration in arid or hyper-arid regions of the same characteristics elsewhere.

Keywords Groundwater exploration · Structurally controlled aquifer · Satellite gravity · Land-based geophysics · Hyper-arid regions · DC resistivity

✉ Khaled S. Gemal
khaledgemal@zu.edu.eg

Article Highlights

- In hyper-arid regions, groundwater exploration needs much effort to overcome the shortage of hydrogeological and paleo-environmental information
- The integrated multi-scale geophysical approach builds a robust geological interpretation in hyper-arid environments
- The space-borne geophysical data sets can act as a preliminary stage for planning high-resolution investigations

1 Introduction

Globally, climatic changes are widely predicted to influence water resources in arid and hyper-arid regions. Therefore, a full understanding of the role of groundwater as a component of the global water resources is essential for managing the scarcity of water in arid regions worldwide, and for vastly improving the sustainable development of water resources for the generations to come. In this context, the Egyptian Western Desert (Fig. 1) represents a typical example of the complexity of land development in a region facing water scarcity. In the regions throughout the world that have similar conditions of aridity and population densities, the groundwater plays a crucial role in providing a water supply for different purposes and sustaining important natural worldly ecosystems (Salako et al.

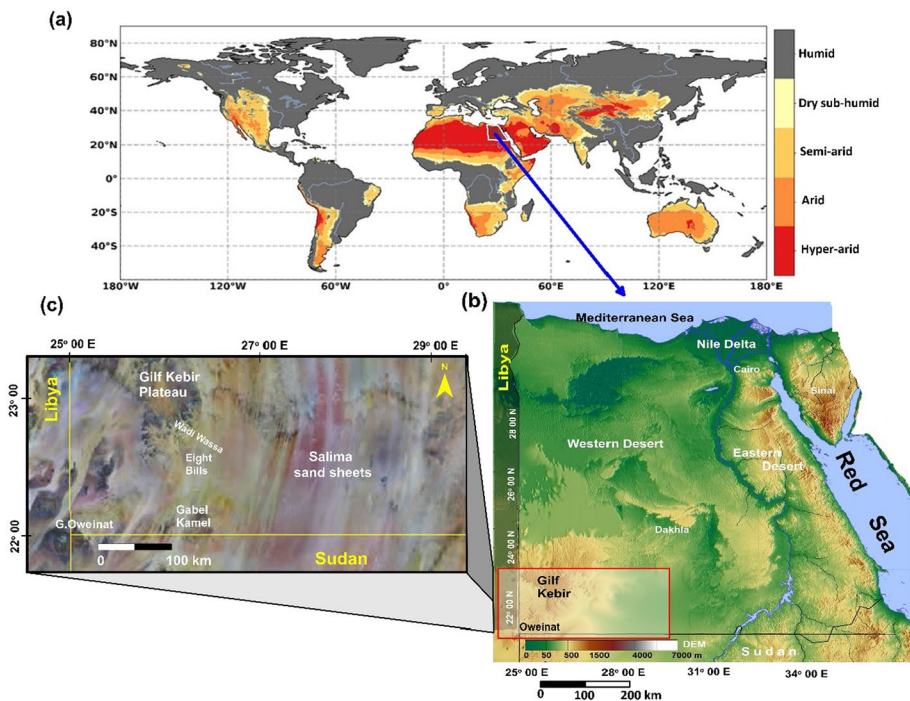


Fig. 1 Location of the study area in the hyper-arid zone. **a** The worldwide aridity map displaying the location of Egypt and North Africa in the hyper-arid zone (Kammerman 2020), **b** Digital elevation model (DEM) map of Egypt and the study area in the southwestern corner, and **c** Landsat image of the investigated area

2009; Famiglietti 2014; Elewa et al. 2016; Wrathall et al. 2018; Bello et al. 2019; Huang et al. 2019). Therefore, exploring and exploiting new sources of groundwater in hyper-arid regions needs much effort (Salem 2015; Mahmoud and Kotb 2017; Abdel Hafeez et al. 2018; Elewa et al. 2021; Khiabani et al. 2021; Gómez-Alday et al. 2022) including assessment of the groundwater potentialities, hydrogeological setting of aquifers, delineation of subsurface structures and their impact on groundwater flow, and the recharge sources (Simmers 1997; Foster and Chilton 2004; El-Meselhy et al. 2020; Herrera et al. 2021; Sahour et al. 2022). Accordingly, the developed exploration programs and sustainable management strategies should be recognized for evaluating the groundwater resources in such regions.

In arid mountainous terrain and very remote regions as in the southwestern corner of the Egyptian Western Desert (Fig. 1), the inspection of paleo-environmental information is an important aspect as the first step toward a realistic and effective design of the groundwater exploration program to overcome the shortage of hydrogeological and paleo-environmental information. According to the current climatic conditions, the area occupies a portion of the hyper-arid zone belt as is characterized by high temperatures (annual mean of maximum temperature: 36.5 °C), and the precipitation is scarce and does not exceed 5 mm/year with an average yearly humidity of 30% and natural evaporation rate of 22.2 mm/d (Mohamed et al. 2022). As a hyper-arid environment, the region has an aridity index exceeding 200, i.e., the evaporation rate exceeds 210 times the precipitation (Gemal et al. 2021a). However, the region has been subjected to previous wet climatic periods in the Early Holocene, which exert their influence on the present surface landscapes and paleo-recharge areas of groundwater aquifers (Kuper and Kröpelin 2006; Sultan et al. 2013).

Unfortunately, the scanty water resources are inherent in such hyper-arid regions and represent a severe problem and a challenging issue for the developmental and economical activities, and give rise to ecosystem degradation and dramatic social repercussions. In such cases, the groundwater conditions in the area represent a key component for any sustainable development strategy in the agricultural activities and urban expansion where the area is not developed and needs much investment that may support the lateral population spread out of the Nile Valley. In addition, the drilled water wells in the eastern border of the considered area (Fig. 1c) have been heavily exploited since the 1990s, which has led to an extensive decline in the potentiometric surface of the Nubian Sandstone aquifer (Ebraheem et al. 2003; Nabawy et al. 2009, 2010; El Alfy 2014; Gemal et al. 2021a and b).

In such arid environments, the Remote Sensing (RS) analysis of satellite radar data (e.g., Radarsat) should be employed as indirect exploration tools to locate the potential zones and basins for groundwater accumulations in hard rocks, and therefore, to identify suitable areas for more detailed field scale surveys (El-Baz 1995; Robinson et al. 1999, 2000; Ghoneim et al. 2007; Laake 2011; Abdelkareem and El-Baz 2015, 2017; Mohammed et al. 2017; Ghoneim and El-Baz 2020). However, none of the previous RS studies in the investigated area has produced complete evidence on the geological structures at a depth that can provide valuable inputs related to the groundwater movement and subsequently locating the potential sites for groundwater exploration. Another important issue is related to the role of deep subsurface structures (faults, fractures, and basement intrusions) in recharging the structurally controlled aquifers as in the case of the Nubian Sandstone Aquifer System (NSAS) that covers the basement rocks in the southern parts of Western Desert. In this aspect, the traditional satellite imagery approach is a great challenge due to the high terrains and extensive sand dunes in these regions, in addition to the innovative data sets that are needed for deep structures detection. Practically, to fill the knowledge gap, in this case, advanced methodologies applied carefully to large scale and high-resolution satellite gravity data in combination with additional data sources (satellite altimetry),

terrestrial geophysical data, and available subsurface geological information can be used to improve the understanding and modeling of the ridge-graben structures in the basement surface (Sander 2006; Braitenberg and Ebbing 2009; Braitenberg et al. 2011; Vaish and Pal 2015; Rabeh et al. 2018).

In recent years, the satellite-based gravity data have been successfully utilized for regional geological mapping of sedimentary basins (Bomfim et al. 2013; Abdul Fattah et al. 2013; Vaish and Pal 2015, Apollinaire et al. 2017; Narayan et al. 2017; Chouhan et al. 2020; Hassan et al. 2021), assessment of groundwater resources (Xie et al. 2012; Ahmed et al. 2014; Singh and Rajuh 2020), and groundwater storage fluctuations (Tiwari et al. 2009; Landerer and Swenson 2012; Sun 2013; Melati et al. 2019). The first decade of the new millennium witnessed the launching of three satellite missions, Challenging Minisatellite Payload (CHAMP), Gravity Recovery and Climate Experiment (GRACE), and Gravity field and Ocean Circulation Explorer (GOCE), which are devoted to gravitational field measurements from satellites with sufficient resolution.

Numerous aspects including the global coverage in addition to the availability and reliability of data quality are the most significant benefits of the space-borne gravity datasets. However, the robust interpretation of satellite gravity data in structurally controlled basins, as any potential geophysical and regional-scale method, needs an additional source of information for an accurate conceptual understanding of the shallow subsurface structures and lateral variations in the composition of sediments and bedrock. Therefore, the combination of multi-scale geophysical techniques, with different physical properties of subsurface layers and water content, can improve the applicability of a single method and reduce the non-uniqueness problem of the interpretation (Gemal et al. 2016).

The advantage of multi-scale geophysical approaches for groundwater exploration has been shown in a number of investigations (Oldenborger et al. 2013; Meier et al. 2014; Parsekian et al. 2015; Muchingami et al. 2021) although applications in arid and hyper-arid regions are rare. In a structurally controlled aquifer such as Nubian Sandstone, the traditional hydrogeological approaches based on available wells are insufficient in these systems where aquifer geometry changes rapidly and unpredictably over small spatial scales. In contrast, the variability in major structural trends and basement reliefs is a critical issue for understanding the spatial variability of groundwater flow paths. Satellite-based gravity data provide regional-scale information of geological structures (Pham et al. 2020; Kumar et al. 2022; Ekka et al. 2022), while at the land scale, ground-based geophysical surveys are applied to describe local changes in sediment or hydraulic properties (Rodell et al. 2007; Parsekian et al. 2015).

Consequently, the overall goal of this research is to explore and develop a practical strategy for groundwater exploration and to study the link between tectonics and groundwater systems in the southern part of the Egyptian Western Desert as a typical example of hyper-arid conditions. For this goal, an integrative and multi-scale approach was applied by utilizing satellite-based gravity data and land-based geophysics including magnetic and DC resistivity measurements as irreplaceable tools to identify the effective faulting trends, which exert a strong control on groundwater flow pathways in the basement surface. This integrative approach also attempts to discriminate between aquifers that hold little or no groundwater potentiality from those having great potentiality. The southwest corner of Egypt, where the Gifl Kebir Plateau is found (Fig. 1), lies within the Dakhla sub-basin of the Nubian Sandstone Aquifer (Mohammed et al. 2017; Masoud et al. 2018; 2019; El Shinawi et al. 2021; Gemal et al. 2021b). The motivation of the applied approach is based on the combination and cross-validation of different geomorphological, hydrogeological, paleo-climate, and geophysical datasets for unraveling the role of subsurface structure

elements influencing groundwater from superficial cover to bedrock at depth in hyper-arid environments. The present research exhibits how integrated multi-scale geophysical data sets with different resolving power produce robust geological interpretation and can be considered as a primary low-cost program for groundwater exploration in regions of extensive aridity worldwide.

1.1 Geological and Hydrogeological Setting

The considered area covers the southwestern part of the Egyptian Western Desert (Fig. 1) as a typical example of hyper-arid environment. From a geological and hydrogeological point of view, several studies have been focused on the impact and origin of geological structures, buried channels, and landforms on groundwater accumulations in the area using remote sensing datasets such as Radarsat (i.e., El-Baz 1998, 2000; Robinson 2002; Ghoneim and El-Baz 2008, 2020; Gaber et al. 2011; Ghoneim 2011; Abdelkareem and El-Baz 2017; Robinson et al. 2017; Masoud et al. 2019).

The Gilf Kebir main plateau covers a large area with an elevation of 1200 m (a.s.l) and consists of two extensive plateaus connected by a small land bridge (Linstädter 2007). The most prominent geomorphologic feature is the prevalence of a fringe of dried and steep-sided valleys with lengths up to 20 km long and 4 km wide that deeply dissect the edges of both plateaus (Linstädter and Kröpelin 2004). An extensive drainage network appears to have progressed primarily from west to east cutting the eastern and southern sides of Kemal El-Din plateau (Fig. 2). To the south of the Gilf Kebir plateau, remarkable conical high hills (Eight Bells) are observed along the NW–SE fault line (Fig. 2). The Eight Bells are related to the widespread volcano-tectonic processes in the area, which have produced

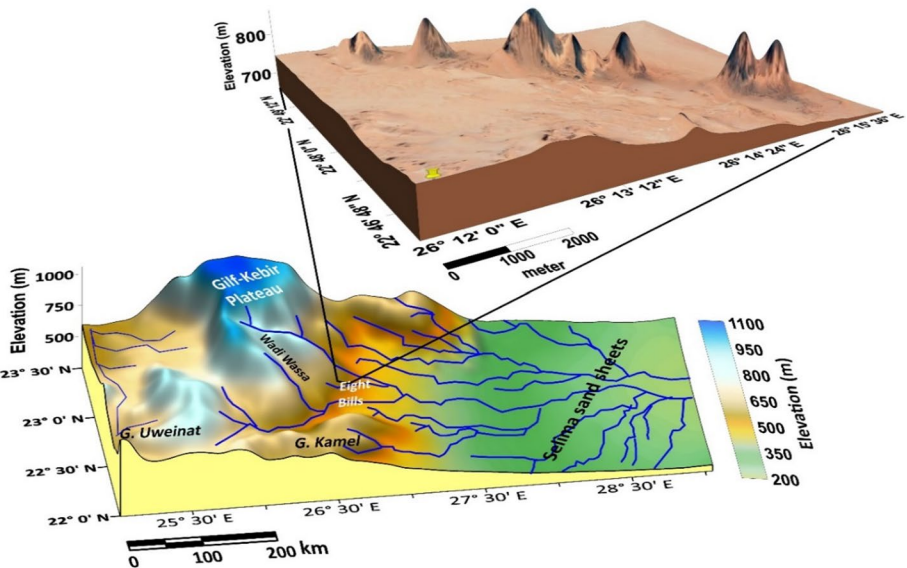


Fig. 2 Three-dimensional topographic block of the extreme southwestern corner of Egypt showing the prominent geomorphologic units and landforms. The drainage network was derived from a DEM (Robinson 2002). The upper block shows remarkable conical high hills along a NW–SW striking line at Eight Bells

crater-shaped structures and dykes (Brügge 2017). Another outstanding geomorphologic feature in the area is Selima sand sheets (Fig. 2) that extend from North Sudan and cover the eastern parts of the considered area for about 250 km (Bubenzer et al. 2020). Its surface is mostly flat with elevations ranging between 200 and 250 m a.s.l, except for the high rocky exposures (500 m a.s.l). Buried stream deposits of fluvial origin were exposed beneath the sand sheet (El-Ghawabi 1987). Ghoneim and El-Baz (2007, 2020) delineated the paleo-watershed in the Selima sand sheets region using the Shuttle Radar Topography Mission (SRTM) and GIS hydrological modeling routine and recognized four main tributaries that drain eastward from Gilf Kebir, Uweinat, and northwestern Sudan highlands (Fig. 2). To the east, the downstream of this mega-basin is characterized by the presence of Late Pleistocene lake deposits (playa) which were favorable for groundwater accumulations during past extreme rainfall events (McCauley et al. 1986; Ghoneim and El-Baz 2007). Robinson (2002) interpreted the high-resolution Radarsat image and Space-borne Imaging Radar C-band (SIR-C) and showed that these paleo-channels are structurally controlled and drain from northwestern Sudan, culminating in the Kharga basin in the northeastern parts of the considered area. Furthermore, the widespread NE and ENE faulting trends and paleo-channels can transport the majority of the water from the south to the Kharga Depression in the north, where it seeps through the underlying fractured sandstone rocks (Robinson 2002). In such conditions, the major faults and fracture zones may connect several sandstone aquifer layers, forming a mega-watershed (El-Baz 1995).

The geological setting in the southwest corner of Egypt is defined by Uweinat–Gilf sub-basin (Issawi and Sallam 2018). Paleozoic rocks have covered the west and east sides of the scarps of the Gilf Kebir Plateau and in the area between the plateau and Uweinat (Fig. 3). In this region, the irregularities in the basement surface are filled with coarse-grained sandstone of Araba Formation (Issawi 1978). In the locality of Uweinat–Gilf sub-basin, a thick sand section (approximately 200 m) was deposited and termed Naqus Formation of Early Silurian (Issawi and Jux 1982). In addition, distinctive sizes of volcanic intrusions of Late Mesozoic–Early Cenozoic Meneisy (1990) are scattered on the surface of the western central section of the Gilf Kebir Plateau. Grolier and Schultejann (1982) believe that volcanic activity ranges in age from Oligocene or Miocene to Quaternary.

The Nubian Sandstone is one of the largest aquifer systems in the world, covering more than 2 million km² in four adjoining countries in the northeastern part of Africa. It comprises three major sub-basins; the most noteworthy is the Kufra sub-basin of around 900,000 km² and expands across Libya, northeastern Chad, and northwestern Sudan (Fig. 4). The second is the Dakhla sub-basin which extends for an area of about 660,000 km² in Egypt, whereas the smallest is the Northern Sudan Platform sub-basin, enclosing an area of around 360,000 m² and is located in northern Sudan (Mohammed et al. 2016). The great majority of the territorial groundwater flow models (e.g., Ebraheem et al. 2003; El Alfy et al. 2014) consider this aquifer as a continual basin. However, the E–W Uweinat–Aswan uplift isolates the Northern Sudan Platform in the south from the Dakhla sub-basin to the north of the area of investigation, while the SE–NW Uweinat–Howar uplift acts as a barrier between Northern Sudan Platform and Kufra basin in the west (Fig. 4). The NSAS comprises, for the most part, water-bearing Paleozoic and Mesozoic sands with silt and clay intercalations of Tertiary sediments of deltaic origin (Thorweihle 1986; Hesse et al. 1987) with different thicknesses of 500, 3000, and 4000 m in the Northern Sudan, Dakhla, and Kufra sub-basins, respectively.

During the last two decades, an intensive drilling program was carried out in the eastern regions of the considered area for irrigation and small domestic purposes. The groundwater is mainly fresh (500–1000 ppm) and satisfactory for drinking and

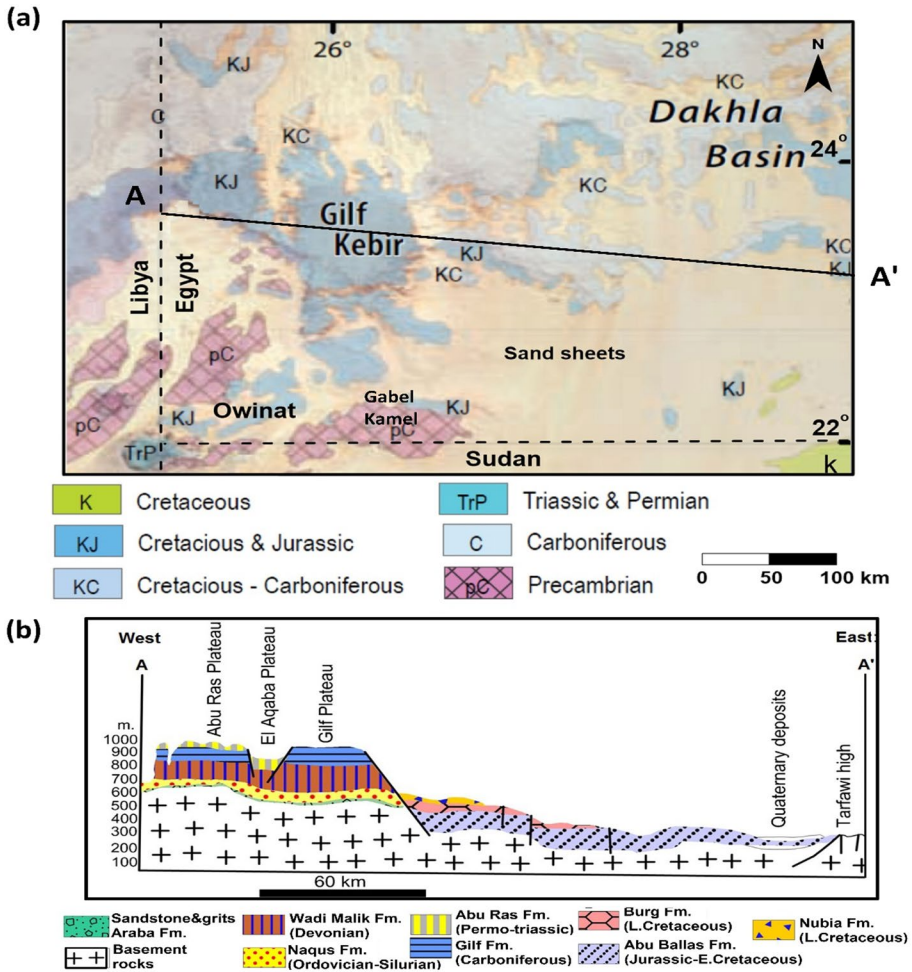


Fig. 3 Geological setting of the considered area. **a** Geological map of the area proximal to Gilf Kebir Plateau (USGS 2002), and **b** geological cross section between Abu Ras Plateau in the west and Tarfawi high in the east (Issawi and Sallam 2018)

irrigation usage (Gemal et al. 2021; Mohamed et al. 2022). The saturated thickness in the drilled wells is highly variable ranging between 137 and 650 m and the depth to the water table ranges from 34 to 58 m. According to Foster and Loucks (2006) and El Alfy (2014), no recent significant groundwater recharge has been detected and the groundwater is non-renewable water (fossil water), thus planning the use or pumping from drilled wells should be based on the probability that sometime in the future the water in these aquifers will be fully depleted. Reasonably, the current research aims to delineate the subsurface structures and reliefs in the basement rocks that have subdivided the area into sub-basins and controlled the aquifer recharge and groundwater movement. Understanding the conceptual flow model in structurally controlled aquifers can be employed to establish a sustainable monitoring policy to manage and prevent intensive use in the

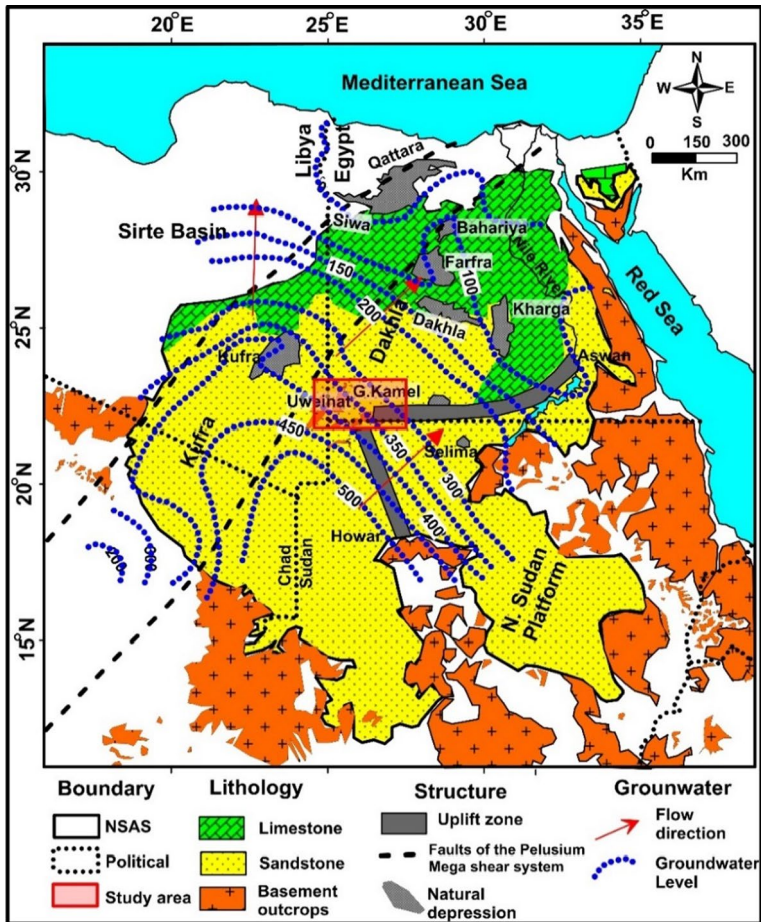


Fig. 4 Location map displaying the sub-basins in the northeastern Africa comprising the Nubian Sandstone Aquifer System (NSAS), the two major basement uplifts (Uweinat-Aswan, Uweinat-Howar), the groundwater level contour lines (above mean sea level) and the groundwater flow directions (modified after Mohamed et al. 2016)

regions of non-renewable sources considering the site characterization and the joint structures.

1.2 Methodology and Data Acquisition

To accomplish the objective of the present study, different geophysical methods have been utilized and arranged in a sequential manner from large to local scale as illustrated in the flow chart in Fig. 5. In this integrative approach, two different high-resolution satellite gravity data sets (EIGEN 6C4 and TOPEX1-min,) were employed to map the entire area's regional geological structures and lithological boundaries. Based on the collected prior regional geological and hydrological information derived from the forgoing investigations and interpretation of satellite gravity and remote sensing datasets, two promising

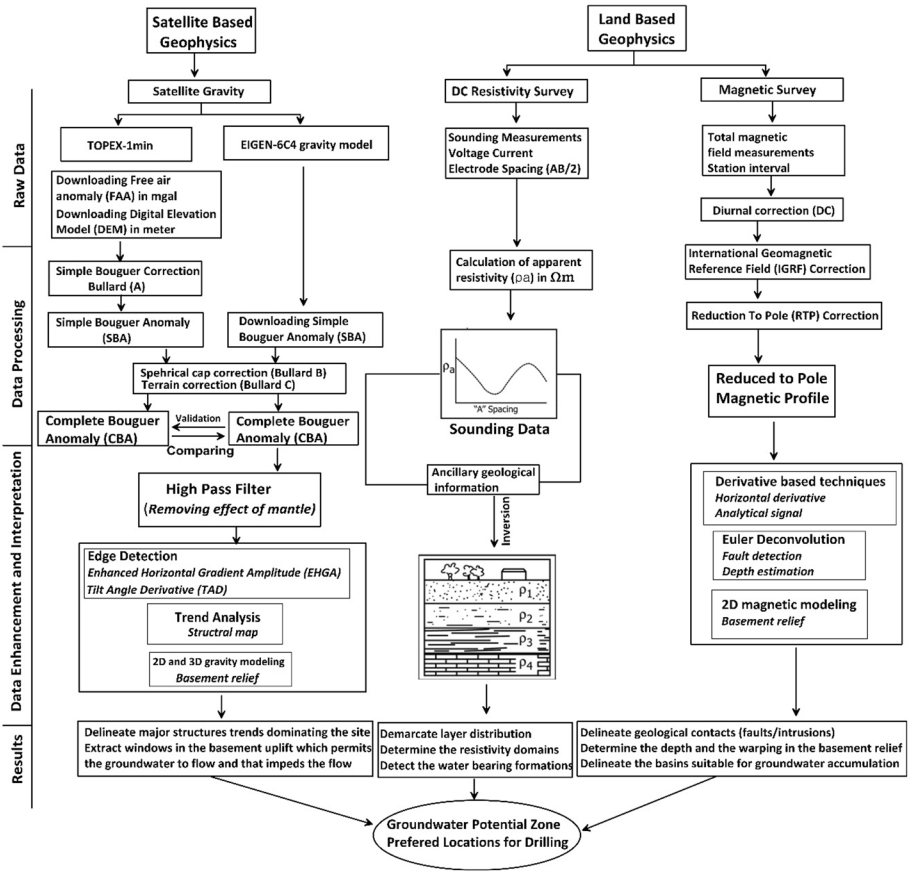


Fig. 5 Workflow of the integrative approach combining satellite and land-based geophysics for locating groundwater potential zones

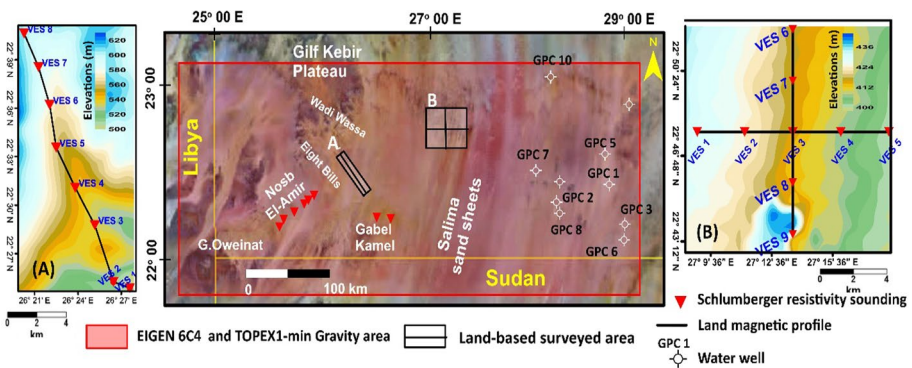


Fig. 6 Geophysical layouts show the available satellite gravity datasets and the land-based geophysical measurements in the two selected sites: **a** magnetic and DC resistivity profile at northwestern Gabel Kamel (south to the Eight Bells), and **b** two crossing profiles (EW and NS, respectively) at northeastern Gabel Kamel

Fig. 7 Shaded relief maps of the available satellite gravity data: **a** the simple Bouguer anomaly map derived from EIGEN-6C4, **b** digital elevation model (DEM) from Topex, **c** Free air anomaly map (FAA), **d** the computed simple Bouguer anomaly map derived from TOPEX-1min

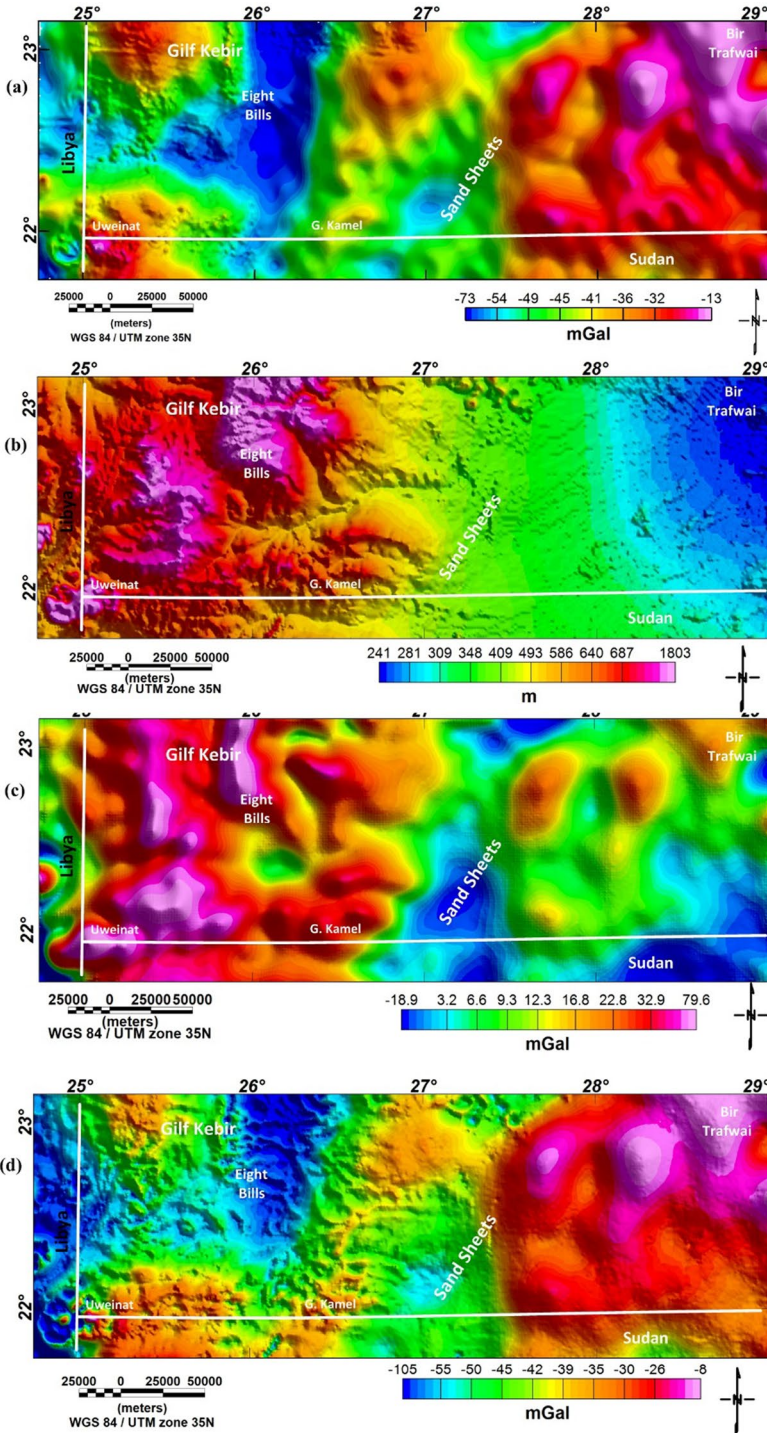
sites, southeast Eight Bells and northeast Gabel Kamel (Fig. 6), were selected for further investigation using land-based geophysical measurements including land-magnetic and DC resistivity measurements. The satellite geophysical dataset and field measurements in the applied approach can be summarized as follows.

1.3 Large-Scale Satellite Gravity Dataset

Firstly, the gravity field data in the form of simple Bouguer anomaly (SBA), based on EIGEN-6C4 model, was downloaded in ASCII-XYZ format from International Centre for Global Earth Models (ICGEM) at GFZ Potsdam (<http://icgem.gfz-potsdam.de>) (Ince et al. 2019). It was sampled to 0.009° (approximately 1 km; the maximum resolution for the EIGEN-6C4), then gridded and displayed in a shaded relief image (Fig. 7a). Anderson et al. (2009), Shako et al. (2013), and Förste et al. (2014) discussed the methodologies used to generate the EIGEN-6C4 gravity field model. It combines gravity observations from satellite (LAGOS, GRACE and GOCE) and DTU ground-based data (Anderson et al. 2009). The recent version of the EIGEN-6C4 model is a superior and more resolvable gravity dataset compared with its precursors and has a resolution of 5×5 arc-minutes, which is equal to 9–10 km on Earth's surface. Additionally, airborne gravity data and GPS observations were used to assess the accuracy of this gravity field model (Shako et al. 2013).

Along with the gravity field model of EIGEN-6C4, the data sets of satellite altimeters GEOSAT and ERS-1 combined with CryoSat-2 and Jason-1 with a grid cell size of 1 arc minute were used (Sandwell and Smith 2009; Andersen et al. 2009; Sandwell et al. 2013, 2014). The datasets of the two altimeters (CryoSat-2 and Jason-1) are characterized by high track density and used to enhance the older altimeter data (Geosat and ERS-1). Topography and gravity field data were downloaded from TOPEX/Poseidon (a geodesy satellite launched by NASA). Satellite gravity data, in the form of free air anomaly (FAA), Version 29.1 together with corresponding geographic location and elevation (Version, 19.1), were downloaded in ASCII-XYZ format from Satellite Geodesy at Scripps Institution of Oceanography, University of California San Diego, USA (http://topex.ucsd.edu/cgi-bin/get_data.cgi), with 1 arc-minute (1.85 km) resolution (Sandwell et al. 2014). The DEM and FAA datasets were re-gridded and plotted in color-shaded relief maps (Fig. 7b, c, respectively) using the Oasis Montaj Program v.8.3 (Geosoft 2015). The gravity effect of the Bouguer slab ($2\pi G\rho h$) was then subtracted from the FAA to produce SBA (Fig. 7d) where the observation points move back down to the datum sea level.

From Fig. 7c, it can be inferred that the FAA map did not reflect the lithological boundaries due to the presence of rugged mountainous terrain particularly in the western part of the investigated area (Fig. 7a). Accordingly, a simple Bouguer (Bullard A) correction was carried out to consider the extra mass located between the observation point and the datum (geoid) in which the landmass above sea level can be approximated by a semi-infinite slab



of uniform thickness and density. Practically, the Bullard (A) correction was implemented using the average density of 2.67 g/cm³ for shallow crustal materials (Li et al. 2007). This value is feasible in the present case study where the main objective is to detect the shallow structures in the sandstone overburden and can change based on the regions and expected depths.

Further corrections were applied to the SBA of EIGEN-6C4 and TOPEX data sets (Fig. 7a, d) to generate the complete Bouguer anomaly. Firstly, the spherical cap (curvature or Bullard B) correction was applied to convert the geometry for the Bouguer correction from an infinite slab to a spherical cap with a surface radius of 166.735 km. Secondly, the terrain correction (Bullard C) was applied where the considered area is characterized by a significant rugged topography in the western parts. The resultant complete Bouguer gravity maps derived from EIGEN-6C4 and TOPEX-1min are shown in Fig. 8.

A profile of Bouguer gravity of EIGEN-6C4 and TOPEX-1min was plotted (Fig. 8c) for a comparative purpose to select a single type from both data sets for further manipulations. Although the two profiles exhibit similar features, the profile of EIGEN-6C4 appears to be much smoother, where the extensive necessary infinite slab and terrain corrections which were applied to TOPEX-1min data might deteriorate the resulted simple Bouguer anomaly map. As a result, the EIGEN-6C4 Bouguer gravity data were considered for further investigation of the area, and the TOPEX-1min data was not examined further. Accordingly, regional–residual separation using high-pass filter, tilt angle derivative, enhanced horizontal gradient amplitude, and 2D forward gravity modeling as well as 3D inversion gravity modeling was applied to delineate the structural boundaries that govern the groundwater flow. Additionally, the enhanced horizontal gradient amplitude (EHGA) method was used for edge detection (Pham et al. 2020). This method is based on the arcsine function and the ratio of the vertical to the total gradient of the HGA.

1.4 Land-Based Geophysics

The geophysical field work commenced by carrying out a magnetic survey that aims to delineate the warping of basement relief topography as well as mapping the major structures (faults, rock discontinuities, intrusion, grabens, and horsts) that might dominate the groundwater potentialities in the area. To validate the gravity anomalies, the magnetic survey was conducted along three long profiles distributed in different directions on both sides of Gabel Kamel NE–SW ridge (one profile northwest Gabel Kamel and two crossing profiles at northeast Gabel Kamel, A and B in Fig. 6, respectively) based on the accessibility of the ground conditions and the initial results of satellite gravity data. Two magnetometers (Proton precision G-856AX with accuracy 0.1 nT and Cesium Vapor G-859Ap with accuracy 0.02 nT) were synchronized for collecting the total magnetic field measurements. Practically, one device was set up at the established base station to monitor the temporal variation in the Earth's magnetic field along with specified time interval and consequently carry out the diurnal and micro-pulsation correction. The base station was selected to be easily accessible and has a very low magnetic gradient. Moreover, it was located away from any natural or manmade magnetic sources and tested to ensure that the background magnetic field is relatively uniform throughout the survey area to be of external origin (Gambetta et al. 2007). A total of 200 magnetic dial readings were collected using the second device with sampling intervals ranging between 100 and 400 m to avoid data aliasing.

For the magnetic dataset, a program of SignProc was used to convert the data to the frequency domain and subsequently carry out further enhancement analysis of the measured

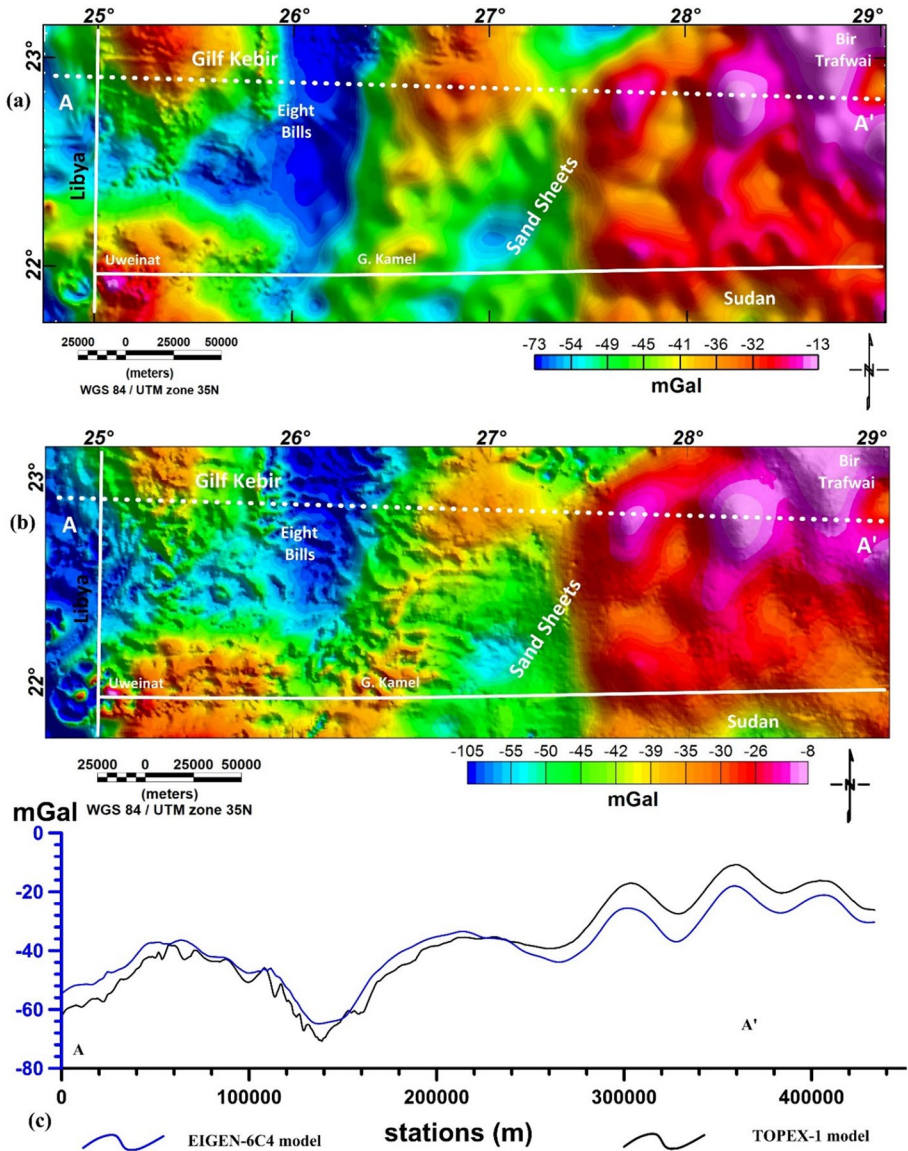


Fig. 8 Comparison between the complete Bouguer anomaly maps derived from **a** EIGEN-6C4 dataset, **b** TOPEX-1min dataset, **c** comparison of plots of EIGEN-6C4 Bouguer anomaly and TOPEX-1min Bouguer anomaly along profile AA', for location see TOPEX-1min map

magnetic profiles. Edge detection techniques such as analytical signal and total horizontal derivative were applied to figure out the true boundaries of geologic contacts (faults, dykes, and intrusions) that are responsible for recharging the aquifers in the area. Furthermore, a semi-automated technique of 2D Euler deconvolution was applied along the measured magnetic profiles using a structural index of 1 to 3 with a step of 0.5 to identify the vertical edges and determine the basement reliefs (Reid et al. 1990). Finally, two-dimensional

magnetic modeling was performed along the magnetic profiles using the GM-SYS program of Oasis Montaj (Geosoft 2015) to outline the fluctuation in the basement surface. The location of faults and the width of the modeled blocks were constrained by incorporating all available prior geophysical and geological information.

Afterward, the diurnal correction was carried out, and to emphasize more local field variations due to crustal sources, the International Geomagnetic Reference Field (IGRF), a global model of the Earth's magnetic field, was subtracted from the measured data. Finally, the reduction to pole (RTP) transform was applied to remove the effect of the inclination angle of the main magnetic field of the Earth. Moreover, the RTP filter helps for adjusting the magnetic anomalies to their real position, where the magnetic anomalies are shifted to the north along the profiles traversed in the south–north direction.

After finishing the magnetic survey, DC resistivity measurements in the form of vertical electrical sounding (VES) were performed using Syscal Junior R2 (IRIS) to confirm the magnetic results and directly map the groundwater potentiates in the area. The method has been recognized to be more suitable for hydrogeological and environmental investigations in different conditions (Iserhien-Emekeme et al. 2004; Alabi et al. 2010; Anomohanran 2011; Gmail et al. 2017; Gouet et al. 2020). A total of 25 sounding points were measured with systematically current electrodes semi-spacing (AB/2) between 1.5 and 1000 m to penetrate the sandstone cover and reach the basement surface based on the available geological and satellite gravity information. The soundings were performed using a well-known Schlumberger electrode layout which is less sensitive to lateral inhomogeneity beside its deeper penetration depth. At the investigated area of southeast Eight Bells (Fig. 6a), eight sounding points were deployed along the profile marked by a dashed black line, whereas the area of northeast Gabel Kamel encompassed two crossing straight profiles comprising nine sounding points and traversing in N–S and E–W directions (Fig. 6b). In addition, eight sounding points were distributed in different places based on the RS and satellite gravity datasets (i.e., Gabel Kamel and Nosb Alamir). During the field works, the standard deviation (SD) errors from repeated cycles together with reciprocal errors were estimated to validate the quality control of readings and excluding artifacts from the measured data. Values of higher standard deviation were eliminated manually. To overcome the aridity conditions shown by the surface layers that are characterized by very resistive ferruginous sandstone, some measures were considered, such as digging a hole for each electrode, adding saline water in the hole and increasing the number of current electrodes on both sides, particularly at large distances. Over and above, the global coordinates of all geophysical data, in terms of northing and easting and topographical data, were acquired using a Trimble G8 GPS system to facilitate locating the favorable zone for forthcoming drilling with high accuracy.

For DC resistivity data, the field measurements (apparent resistivities and AB/2) at each site were inverted to determine the vertical layer distribution using IPI2win program (Bobachev et al. 2008). This inversion scheme is based mainly on the linear filtering algorithm, which creates a rapid and accurate direct problem solution for a wide range of models, involving all the reasonable geologic and hydrogeological situations (Gemail 2015). In addition, Occam's inversion was applied to find the smoothest model which fits the data to an approved tolerance (Vedanti et al. 2005). Figure 9 shows an example of the geological interpretation and Occam's inversion of sounding points VES1 and VES3 at NE Gabel Kamel.

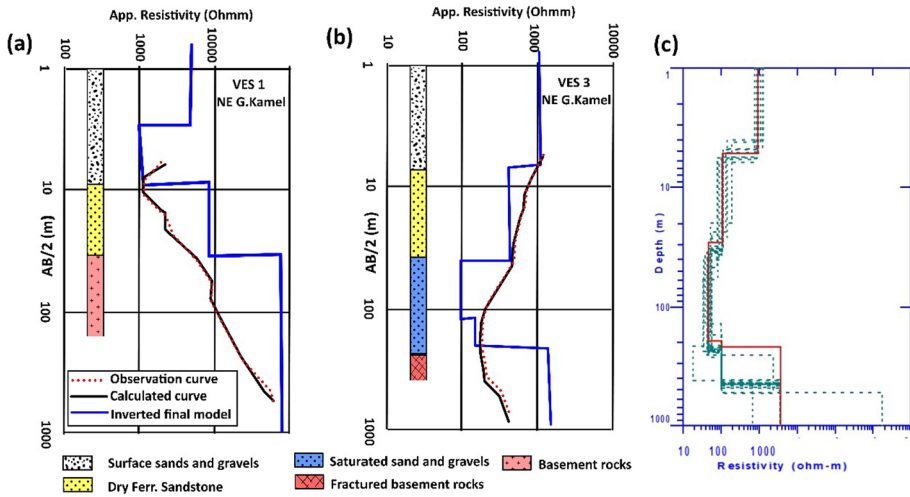


Fig. 9 Example of geological interpretation of two sounding points at NE Gabel Kamel **a** resistivity curve at VES1 indicates shallow basement at 45 m depth and dry sandstone overburden, **b** resistivity curve at VES3 displays a promising sandstone aquifer at 40 m depth with 250 m thickness, **c** interpretation of VES3 using Occam’s inversion and equivalence analysis

2 Results and Discussion

2.1 Satellite-Based data

2.1.1 Comparison of Bouguer Anomalies and Geological Map

The derived Bouguer anomaly map was visually inspected in terms of boundaries between lithologic units with different densities, constrained by the surface exposures where available (Fig. 8a). The anomaly values were qualitatively tied to definite lithology; consequently, the gravity data was used as complementary information in delineating the boundary of each rock type. It is a clear evidence that the polarities of the Bouguer gravity values are negative and the amplitude ranges from -73 to -13 mGal. To ensure the accuracy of the corrected Bouguer map (Fig. 8a), the derived anomalies were qualitatively correlated with the in situ geological and geomorphologic features as indicated in the surface geological map (Fig. 3) and Landsat image of the area (Fig. 1c). In the complete Bouguer anomaly map (Fig. 8a), the influence of the basement outcrops at Gabel Uweinat and Gabel Kamel in the southern boundary is expressed by high Bouguer gravity values (-13 and -36 mGal, respectively). Contrarily, Selima sand sheets to the east of Gabel Kamel can be traced by their well-defined gravity lower signal than the surrounding uplifted basement at Trafawi high in the eastern boundaries of the area (Fig. 8). Additionally, pronounced negative anomalies extend in the NS direction, passing through the Gilf Kebir plateau with minimum amplitudes (-73 mGal), may indicate a thick sedimentary sequence in a local basin. Linear Bouguer gravity anomalies denote regional structures mostly faults and uplifts, where the area is structurally complicated by mega-tectonic elements. The eastern part is marked by well-defined isolated anomalies with moderate-to-high gradients, irregular patterns, and

different sizes and shapes. These anomalies could be attributed to the shallow high-density basement and/or basaltic intrusions.

The complete Bouguer gravity map, derived from EIGEN-6C4, was analyzed using a high-pass filter to extract the effect of the Nubian Sandstone in the investigated area, where the deep mantle contributions were removed from Bouguer anomalies using a cut off wave-number: 0.01 Rad/m (Obenson 1974; Block et al. 2009, as shown in Fig. 10a). Figure 10 illustrates the regional–residual field separation obtained by high-pass filtering. The overall anomalies values are significantly low, ranging from -15 to 21 mGal (Fig. 10b). The major and distinct geological signatures in the high-pass filtered gravity map correlate well with the existing geological map (Fig. 3).

2.2 Buried Deep Hydro-structures and Aquifer Configuration

As previously stated, the mega-watersheds and numerous buried streams in the area are governed by regional faults and paleo-channels that extend for tens of kilometers and possibly indicate the presence of multiple intersecting horizontal groundwater aquifers. There are minor fault types that act as local pathways of more limited areal extent (Robinson 2002; Ghoneim et al. 2007; Ghoneim and El-Baz 2020). In such case, the faulting system in the area controls the basement reliefs that define the palaeo-channels with sharp boundaries, as well as the thickness of the Nubian Sandstone cover. Therefore, the Bouguer gravity map was filtered using the tilt angle derivative (TDR) method that has much more advantage over other edge detection techniques in accentuating shallow and deep structures equally, moreover delineating the edges of dominant features (Miller and Singh 1994; Verduzco et al. 2004; Oruc 2010; Ekinici et al. 2013; Pham et al. 2020). The TDR is an arctan function of the estimated vertical derivative of the gravity field divided by its total horizontal gradient (Pham et al. 2020). It usually yields the location of faults and contact features more accurately than the first vertical derivative. Moreover, it traces the alignments of deep-seated structural or faulted orientation, which is well-consistent with the regional tectonics (Oruc and Keskinsezzer 2008). The inspection of the TTDR-derived map (Fig. 11a) clearly identifies the structural framework of the shallow basement rocks that are covered by the Nubian Sandstone sequence. Qualitatively, the positive TDR values (violet color; Fig. 11a) may be interpreted as uplifted blocks or intrusion from high-density material. Four positive zones can be easily recognized; in the west of Gilf Kebir (at Egypt-Libya border), G. Uweinat uplift to the southwest, G. Kamel NNE-SSW ridge, and in the eastern part where the basement is exposed to the surface in the northeastern corner near Bir Trafawi uplift (Fig. 11a). These ridges are alternated by negative TDR domains aligned EW, NS and NE. The major negative gravity anomalies trending generally in E–W and N–S directions and locally NNE–SSW to the east of Gabel Kamel suggest deep-buried channels or sub-basins in the sedimentary cover and extend downward in the basement. Zero TDR value (solid black lines; Fig. 11a) that can be identified as light yellow color are coincident or close to edges/contact of the geologic structures. The boundaries derived from the TDR map are compatible with the exposed basement boundaries in the Uweinat and Gabel Kamel areas in the southwest and Bir Trafwai in the northeast corner.

Despite the fact that groundwater flows from the southwest to northeast, its depletion in the southern parts of the Dakhla sub-basin is seemingly attributed to the presence of EW Uweinat-Aswan uplifting, which inhibits the groundwater flow and consequently reduces replenishment from the southern recharge areas (Hesse et al. 1987; Mohammed et al. 2016). However, the NS and NNE paleo-river courses and the bounded faults in the

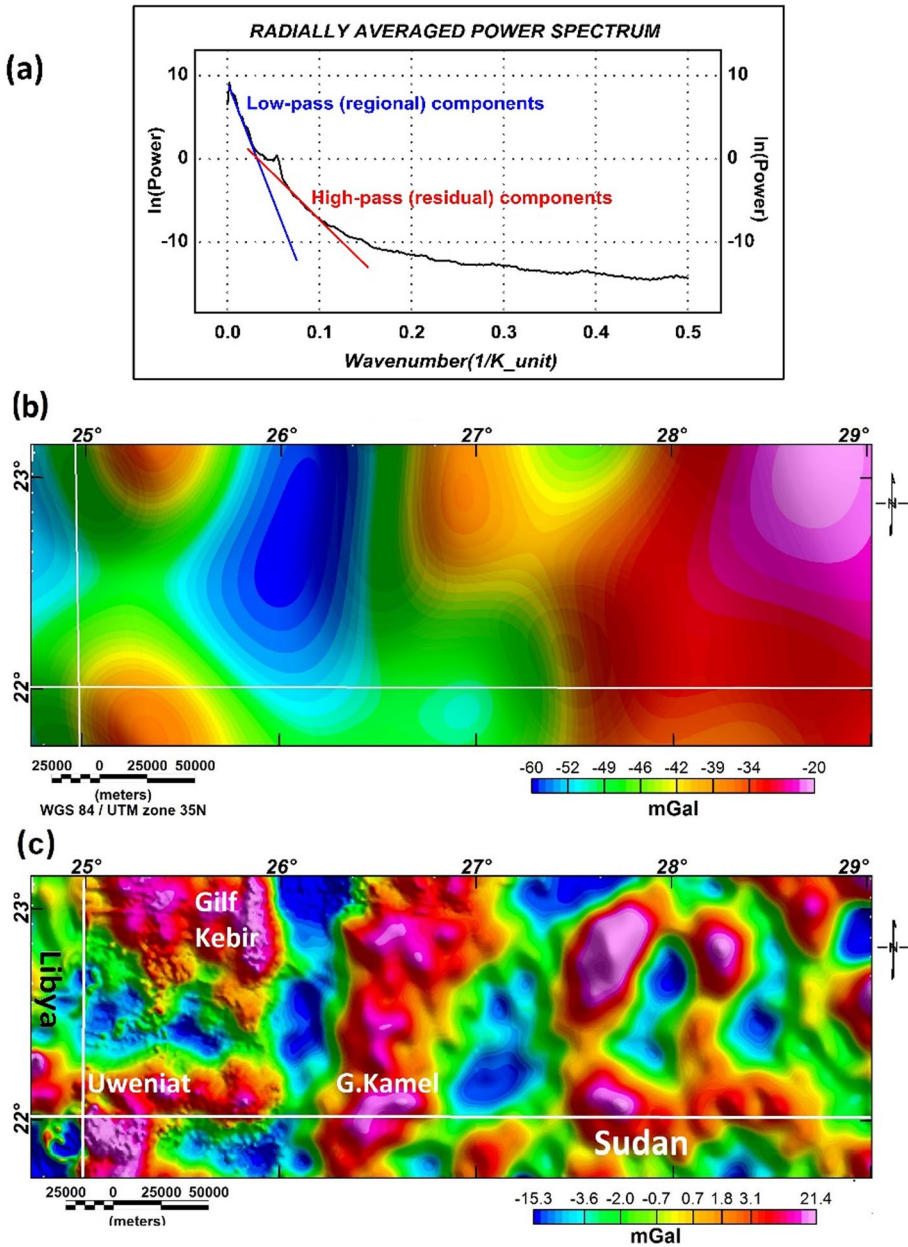


Fig. 10 Regional and residual gravity anomalies separation using high-pass filtering, **a** radially average power spectrum curve of the complete Bouguer anomaly map identifies two linear segments; the blue segment denotes the long wavelength anomalies from deeper sources, whereas the red one represents short wavelength anomalies of shallower sources. **b** Regional gravity map, **c** high-pass filtered gravity map

Fig. 11 Comparison between the derived gravity anomalies and the superimposed drainage patterns from ▶ Radarsat-1 and SRTM, **a** tilt angle derivative (TDR) map of the Bouguer gravity anomaly. Solid black lines represent zero contour, **b** the paleo-drainage system (Ghoniem and El-Baz 2020) superimposed on high-pass filtered gravity map, and **c** the interpreted drainage features and alluvial fans overlain on SRTM-derived slope map showing the role of NE and ENE structural trends in recharging the local aquifer during the Early Holocene (Robinson et al. 2007)

area east of Gabel Kamel as detected from the TDR and high-pass filtered gravity maps (Fig. 11a, b, respectively) are thought to be good groundwater conduits that connect the Nubian Sandstone overburden with the recharging aquifer in northwestern Sudan. Moreover, it acts as a preferential flow path and controls the flow of the groundwater from the south to north and northeast direction. To validate this assumption and understand the role of these mega-structures in aquifer configuration, the results obtained from the derived TDR and high-pass filtered maps were correlated and integrated with the previous results from Radarsat-1 and SRTM and other optical remote sensing data (Robinson et al. 2000, 2007; Ghoneim et al. 2007; Ghoneim and El-Baz 2008, 2020).

Robinson et al. (2007) delineated a closed basin east of the Gabel Kamel (Fig. 11c), based on multispectral and Radar SIR-C images where the Selima sand sheets lie that receives water from the surrounding southern highlands. Additionally, Robinson et al. (2007) constructed new fluvial and slope maps of southwest Egypt (Fig. 11c) based on SAR data and delineated the alluvial fans and buried channels at the eastern edges of Gilf Kebir plateau. The correlation of these remote sensing observations with the high-pass filtered and TDR maps indicates that the area could be discriminated into two different geological provinces around the N–S ridge of Gabel Kamel (Fig. 11a, b). Interestingly, the area east of Gabel Kamel is intersected by several northeast drainage lines that extend from northwestern Sudan and open the southern E–W Uweinat-Aswan uplift (Fig. 11). In contrast, the western side is characterized by E–W and NNE–SSW structures that likely brought water from the western tributaries during monsoon periods in the Early Holocene (8500–7000 B.C.E).

2.3 Faults and Groundwater Recharge System

From the hydrogeological standpoint, the inspection of gravity lineaments and bounded basement faults is critical for understanding how the aquifer system in the area of investigation is recharged. The recent high-resolution edge detection technique of enhanced horizontal gradient amplitude (EHGA) was calculated to define the major fault trends controlling the pathway of groundwater in the area (Fig. 12a). It provides more accurate and better resolution edges, as well as avoids false edges in the results (Pham et al. 2020). The EHGA map (Fig. 12a) exhibits sharp quasilinear and continuous structures associated with abrupt density changes as peaks of maxima horizontal gradient. Alternatively, the major and distinct lineaments are graphically plotted on the areas of the high gradient of tilt derivative values. The extracted lineaments are superimposed on the tilt derivative image (Fig. 12b) and show a strong correlation with that of EHGA.

Examination of the extracted lineaments from the EHGA- and TDR-based approach (Fig. 12a, b) reveals that the N–S and E–W are the dominant major trends in the western region (west of Gabel Kamel rose diagram, Fig. 12b) which control the subsurface structures and correlate well with the presence of basement exposures at Gabel Uweinat and Gabel Kamel. The southern extensive E–W faults along with the uplifted basement act as natural barriers in the direction of water flow from northwestern Sudan. Therefore,

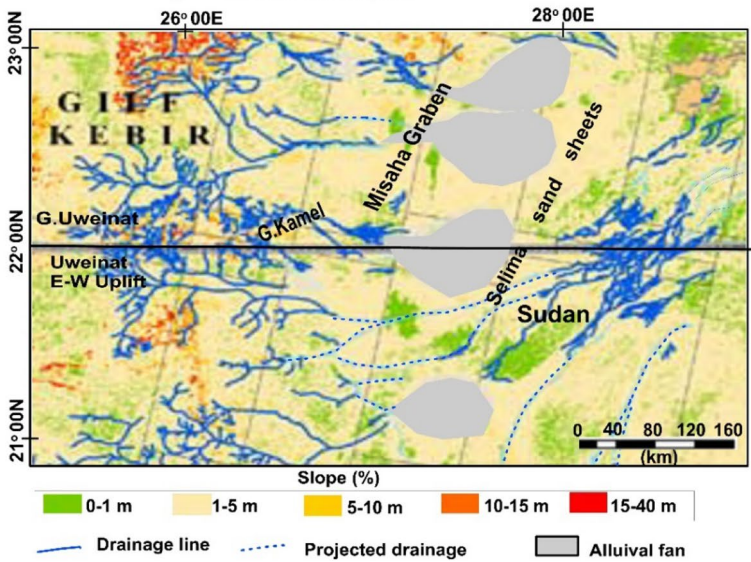
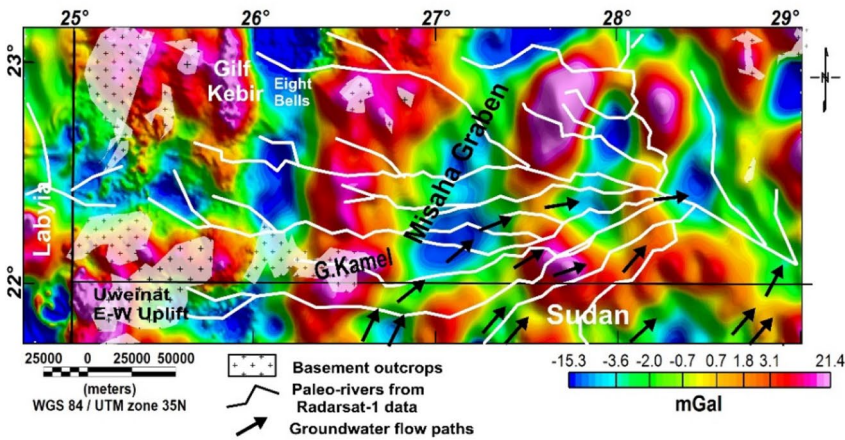
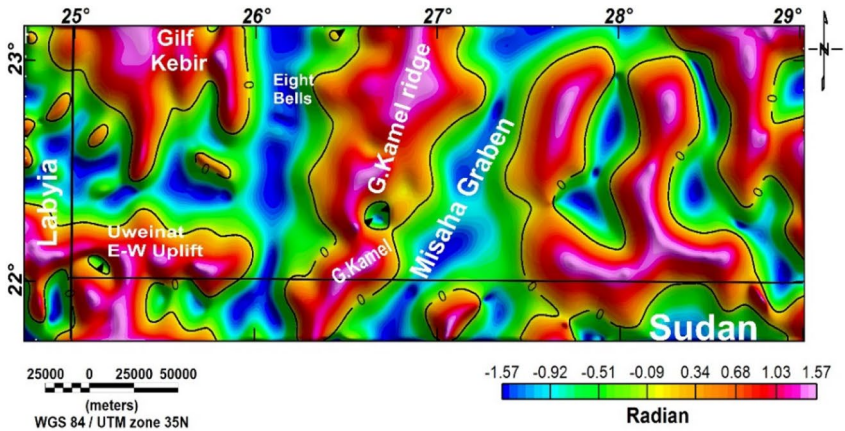


Fig. 12 Lineaments extracted from **a** edge detection technique of enhanced horizontal gradient amplitude (EHGA), **b** TDR map and rose diagrams in the west and east sides of Gabel. Kamal, and **c** lineaments map of northwestern Sudan and Southwestern Egypt (Mansour 1991) derived from Landsat image and the monsoonal rain in Early Holocene (Kuper and Kröpelin 2006)

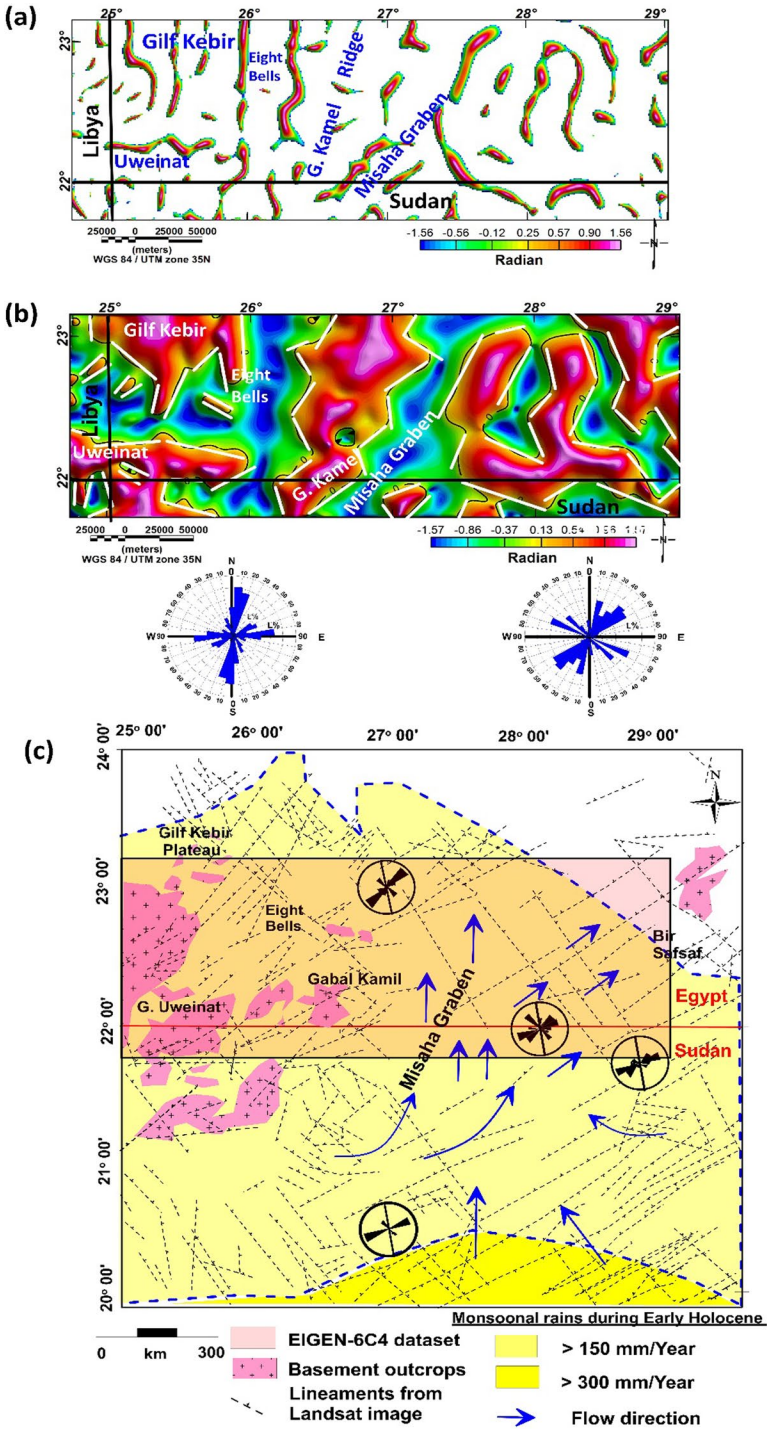
these faults reduce the occurrence of groundwater along with the crossing S–N trend in the area due to shallow basement reliefs. In addition, the controlling E–W faults in the western part of the area could explain the abundance of E–W paleo-channels that facilitated the water flow during wetter periods (8500–7000 B.C.E) from western high mountainous terrains to east Uweinat lowlands as inferred from multispectral and Radar SIR-C images (Robinson et al. 2007; Ghoneim et al. 2007; Ghoneim and El-Baz 2020). In contrast, the NE–SW, NNE–SSW and NW–SE regional trends are the prevailing faults in the eastern regions (rose diagram of east Gabel Kamel, Fig. 12b). These fault trends are most probably controlled by subsurface structures that have an impact on groundwater movement and the aquifer configuration in the eastern regions (Fig. 12). Consequently, the characterization of subsurface structures that control groundwater flow (paleo-rivers) using the lineaments extracted from the derivatives of satellite-based gravity data and RS observations provide insights to identify the groundwater potentialities in addition to better understanding the water flow regime during the wetter periods in the Early Holocene as shown in Fig. 12c. At that time (8500 B.C.E), the current hyper-arid conditions were replaced by savannah-like environments, and the area was receiving a huge amount of monsoon rains from the south (Kuper and Kröpelin 2006).

Based on the lineaments map (Fig. 12), the magnitude and the pattern of the gravity lineaments derived from TDR and EHGA techniques reflect the tectonic framework of the area. The complex pattern of the Bouguer anomaly indicates that the area is characterized by major and minor faults. The composite rose diagram (Fig. 12b) depicts five pronounced major trends arranged in decreasing order according to their abundance: N–S, NE–SW, NW–SE, EEN–WWS, and NNE–SSW. These results correspond to those inferred trends by Mansour (1991) and Robinson et al. (2007) who detected faults with four main directions, namely E–W, N–S, NW–SE, and NNE–SSW (Fig. 12c).

2.4 Basement Relief and Groundwater Potentialities

To verify the gravity lineaments and subsurface basement relief that govern the groundwater potentialities in the area, 2D forward modeling along AA' profile (Fig. 13) of the high-pass filtered gravity was applied to configure the basement surface in the southern border of the area where the depth to the basement fluctuates. The constructed model shows the topmost sedimentary cover with an average density of 2.60 g/cm³ (Senosy et al. 2013) underlain by basement rocks with an average density of 2.8 g/cm³ (Gaulier et al. 1988; Marsouk 1988; Saleh et al. 2006). The available data from four wells (GPC-7, GPC-9, Awkaf 13, and R21 wells) in the east were utilized to constrain the modeling process and to narrow down the possible solutions to a unique plausible geological model. The maximum depth to the basement is 710 m below the ground surface as extracted from the constructed model and forced by GPC-7 well (Fig. 13). Along the model, the basement surface and width of the modeled blocks are changed in an iterative way until achieving an acceptable fit between the observed and calculated anomalies (RMS error = 0.258 mGal).

The examination of the model shows that along the areas proximal to the western uplifting zone, the total thickness of Nubian Sandstone ranges from less than 50 m to nearly



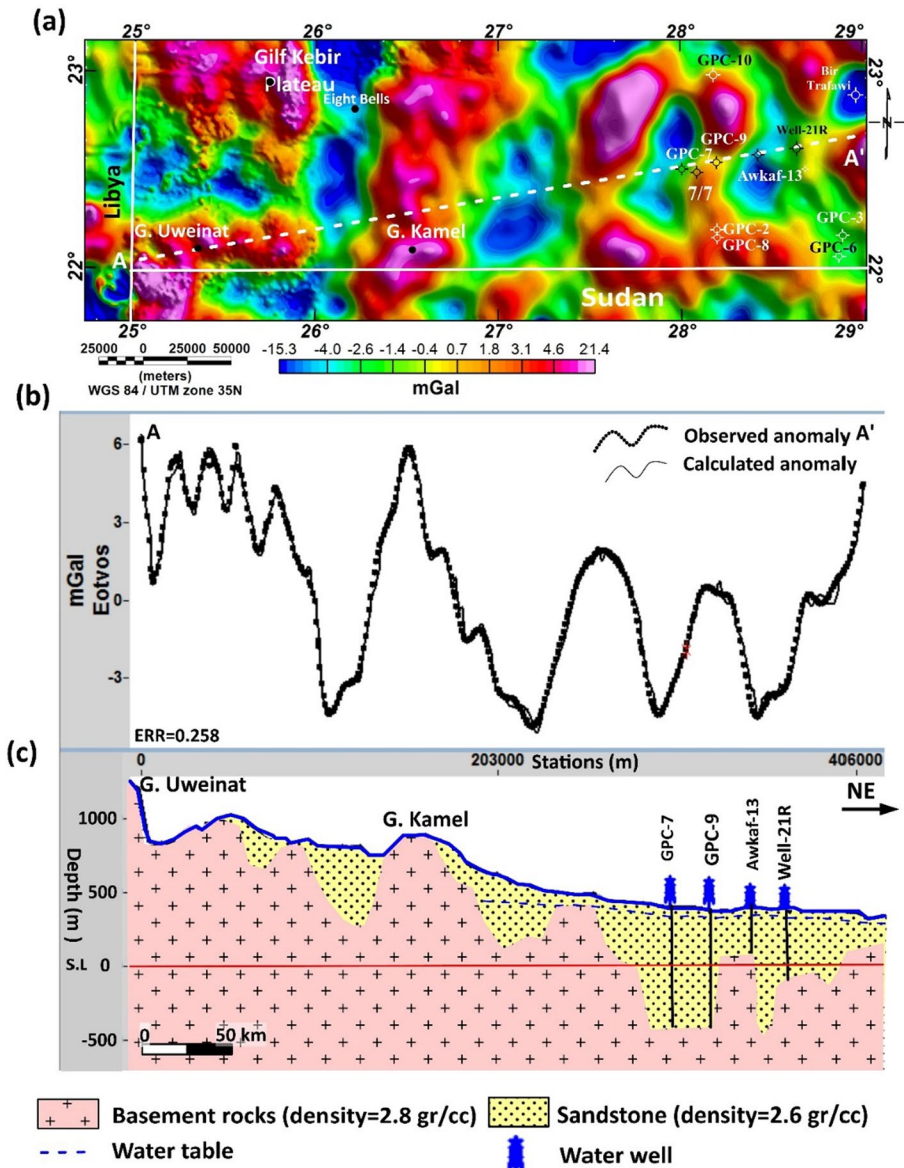


Fig. 13 2D forward modeling along AA' profile **a** high-pass filtered Bouguer gravity anomaly map shows the location of A–A' profile, **b** observed gravity anomalies along AA' profile, and **c** geological interpretation along AA' profile showing the irregularities, and concavities in the basement surface along both sides of Gabel Kamel constrained with four water wells.

375 m, whereas the basement rocks crop out at Gabel Uweinat and Gabel Kamel. It can be noticed that the groundwater flow from the south is blocked along large segments of the Uweinat-Aswan uplift, particularly in areas where the depth to the basement is shallower than that of the groundwater level (Fig. 13). Moreover, the deviation in the direction of

groundwater flow from southwest–northeast to east–northeast could be in part related to the presence of Uweinat–Aswan uplift. This suggestion is supported by the presence of out-flow of some springs (e.g., Bir Trafawi and west Bir Trafawi springs) in the northeastern corner of the area. In addition, the model depicts depressions or windows with a depth to the basement of more than 300 m, which exceeds the water table depth (30–50 m) implying that the groundwater flow is not fully obstructed along the entire length of the uplifting zone. The largest segment is clearly observed to the east of Gabel Kamel (Fig. 13c) and serves as a preferred conduit for groundwater flow, giving the areas directly located northward a hydrological significance. Furthermore, this promising area is considered a part of Misaha Graben which extends, from the eastern side of Gabel Kamel in the west to Bir Safsaf basement rocks in the far East, approximately 350 km long (Fig. 12c).

A 3D inversion gravity modeling was applied to delineate the basement surface. This inversion method is more dependable than that of the forward modeling where the quantitative solutions resulting from inversion are more readily than the iterative trial-and-error process of forwarding modeling (Saibi et al. 2021). The 3D gravity inversion was used to construct a 3D model of subsurface basement depth from topographic and high-pass gravity data using the 3D GM-SYS of Oasis Montaj Ver.8.3.3 (Geosoft 2015). Details on the inversion technique are available in Li and Oldenburg (1996), Touthmalani, and Saibi (2015a, b) and Saibi et al. (2021). The 3D inversion modeling is significant as a guide to show where and how the basement boundaries of the 3D geological model may control the groundwater movements in the area. The applied 3D geological model was constrained by the drilled wells in the eastern region and the estimated depths to the basement surface from land-magnetic and DC soundings in the western area.

The constructed basement relief map (Fig. 14) exhibits a closed basin in the western area west of Gabel Kamel. Contrary, open to semi-open basins (denoted by green color) are located in the eastern area east of Gabel Kamel. In contrast, the basement rocks are exposed and are very shallow (violet to red colors) in the western portion except for the enclosed basin (denoted by the yellow color), which is located south of the Eight Bells.

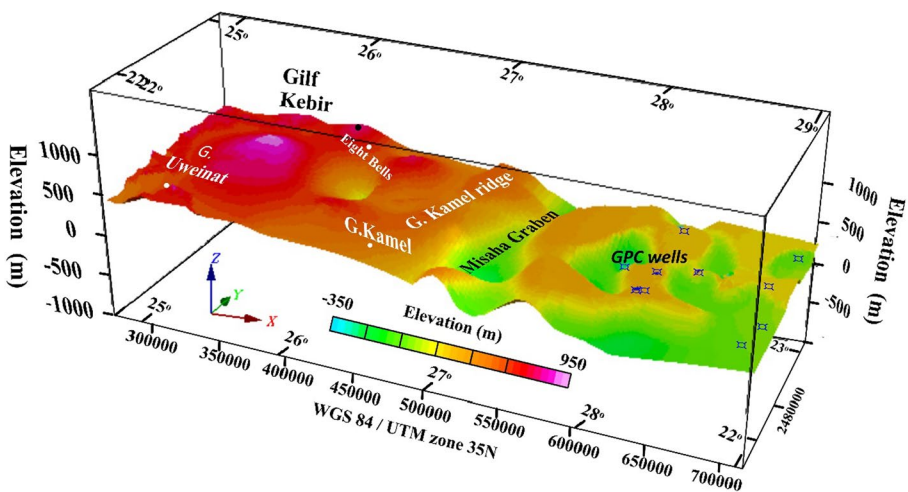


Fig. 14 Extracted 3D inversion gravity modeling shows the basement relief constrained with available wells in the eastern parts and the results of DC resistivity sounding and magnetic methods around Gabel Kamel ridge (coordinates WGS 84/UTM zone 35N)

Otherwise, deep basins (from -500 to 200 m denoted by green color) are divided by shallow basement barriers (from -100 to 200 m denoted by the orange color) characterize the eastern half of the study area.

A structural map was prepared based on the high-pass filtered gravity data (Fig. 15a). To better understand the impact of subsurface structural control on groundwater potentialities and water flow patterns, a 3D block was constructed and compiled from the plane view of the structural map (Fig. 15). Two cross sections were created from 2D gravity modeling along N-S and W-E profiles and boreholes information in the East Uweinat region (Fig. 15b). For instance, the structure map (Fig. 15a) enabled tracing the main tectonic features and the controlling peculiarities of the groundwater flow in the area, especially a boundary between the uplifted basement and Nubian Sandstone. From this perspective, the NNE and NE structures at various spatial scales interrelate with the recharge system from

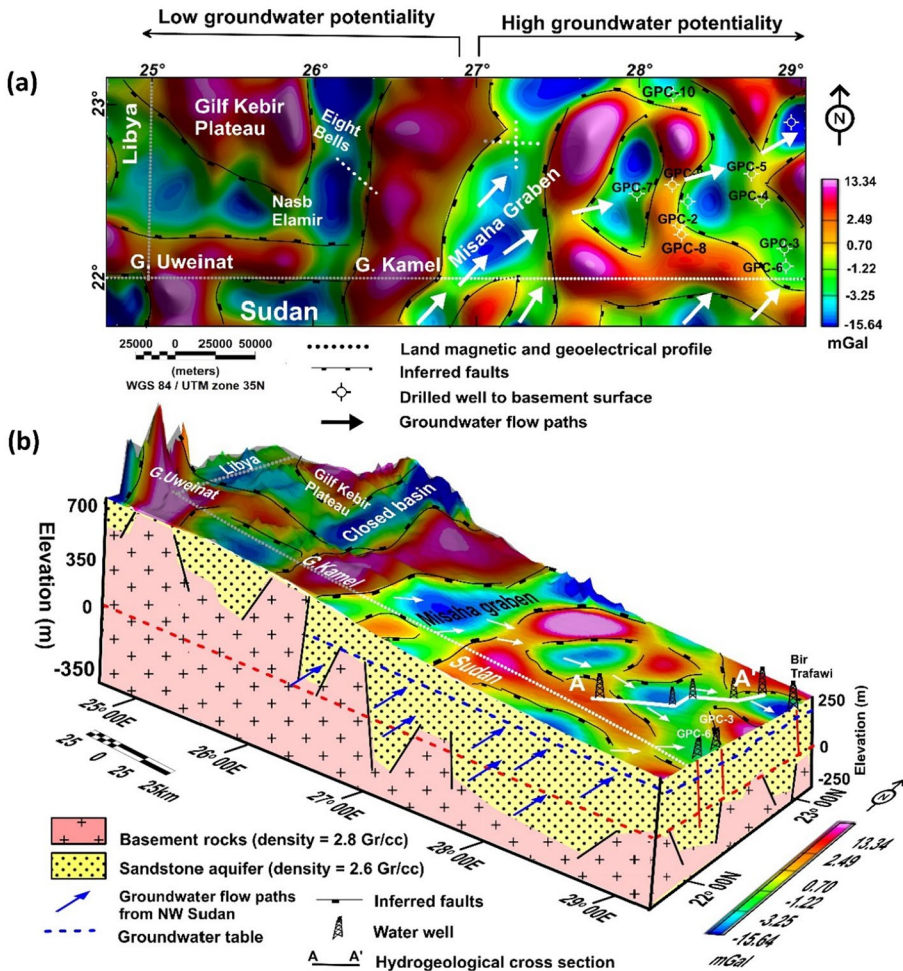


Fig. 15 Extracted structure map from high-pass gravity dataset **a** the major structural elements that control the groundwater potentialities in the area, and **b** a 3D block shows the groundwater flow regime related to the structure elements in the area. The southern and eastern borders of the block were constructed using 2D gravity modeling and constrained with available wells in the eastern side of the area

northwestern Sudan to control the direction, magnitude, and stability of the flow regime in the area east of Gabel Kamel (Fig. 15b). In contrast, the presence of Uweinat-Aswan uplift at shallow depths to the west of Gabel Kamel reduces the groundwater potentialities in the western buried channels and sub-basins. To confirm these results, the geophysical logs and lithologic information from the drilled wells in the eastern side were employed to construct a hydrogeological cross section along the NE profile (Fig. 16). Along this section, the basement surface displays a vertical displacement of about 150 m in a short distance between Awkaf-13 and Awkaf-1 wells, consequently increasing the aquifer thickness to its maximum value in Awkaf-1 well. Therefore, the saturated thickness of the Nubian aquifer varies between 90 m in the northeastern corner near Bir Trafawi to 650 m at GPC-7 in Misaha basin (Ebraheem et al. 2003). The aquifer in these wells is mainly composed of sandstone with siltstone lenses in places.

2.5 Land-Based Data

To validate the results of satellite gravity, two sites were selected for land-based geophysical surveys on both sides of the Gabel Kamel ridge which is a key structural control in the area. The land-based magnetic survey was analyzed to delineate the local structural framework affecting the thickness of the groundwater aquifer in the investigated sites. On the other hand, the vertical electrical sounding results were directed to assess the aquifer potentiality and water quality in the area.

The interpretation of sounding points in terms of true resistivities and actual thickness was used to establish the geoelectric cross sections and subsequently delineate the aquifer layer, if present. The first profile (35.7 km long) was measured on the northwestern

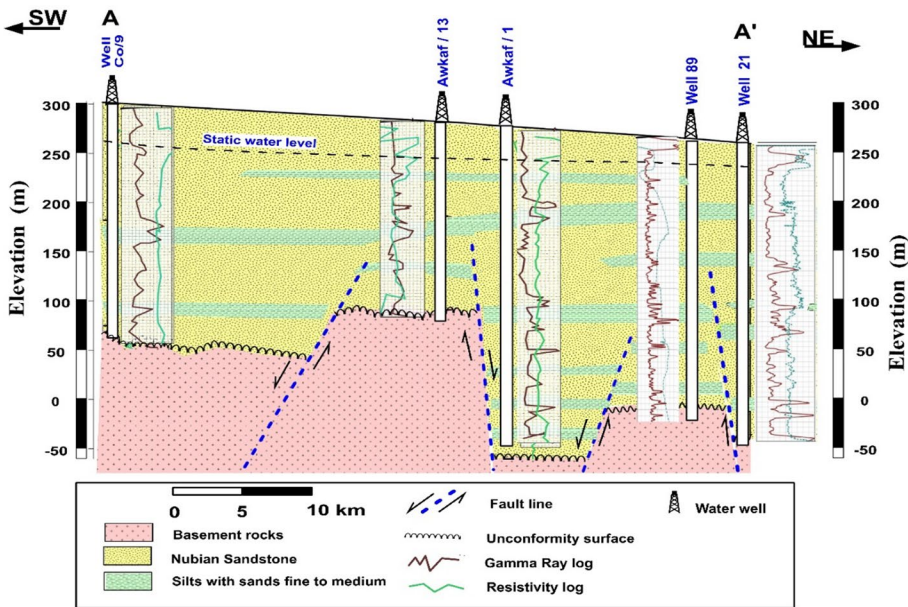


Fig. 16 Hydrogeological cross section from the lithologic and geophysical logs of the drilled wells in the eastern areas. The lithologic description and logs are reported by the Research Institute for Groundwater (for location see Fig. 15b)

side of Gabel Kamel (southeast Eight Bells) intersecting the well-defined N–S sub-basin as indicated from satellite gravity touching the Gabel Kamel ridge in the east (Fig. 15a). Figure 17 displays the results magnetic survey in the form of graphical plots of the applied derivatives and 2D modeling, in addition to the geoelectric cross sections for integration.

The magnetic field varies from -161 to 31 nT with a gradual increase toward the northeast. The results of different derivative techniques (Fig. 17a) exhibit a good correlation between peaks and troughs along with the magnetic profiles, where the edges of faults and boundaries of the magnetic sources are defined by the maxima (peaks) of the analytical signal (Fig. 17a) and the high amplitude of total horizontal derivatives. The 2D magnetic model (Fig. 17b) depicts seven polygons (P1 through P7) with magnetic susceptibility varying from 0.0004 to 0.0033 , in CGS units, reflecting acidic to intermediate basement rocks. Close examination of the model (Fig. 17b) reveals that the maximum thickness of the sedimentary basin is located at the central part reaching about 1200 m and decreasing dramatically toward both ends of the profile reaching

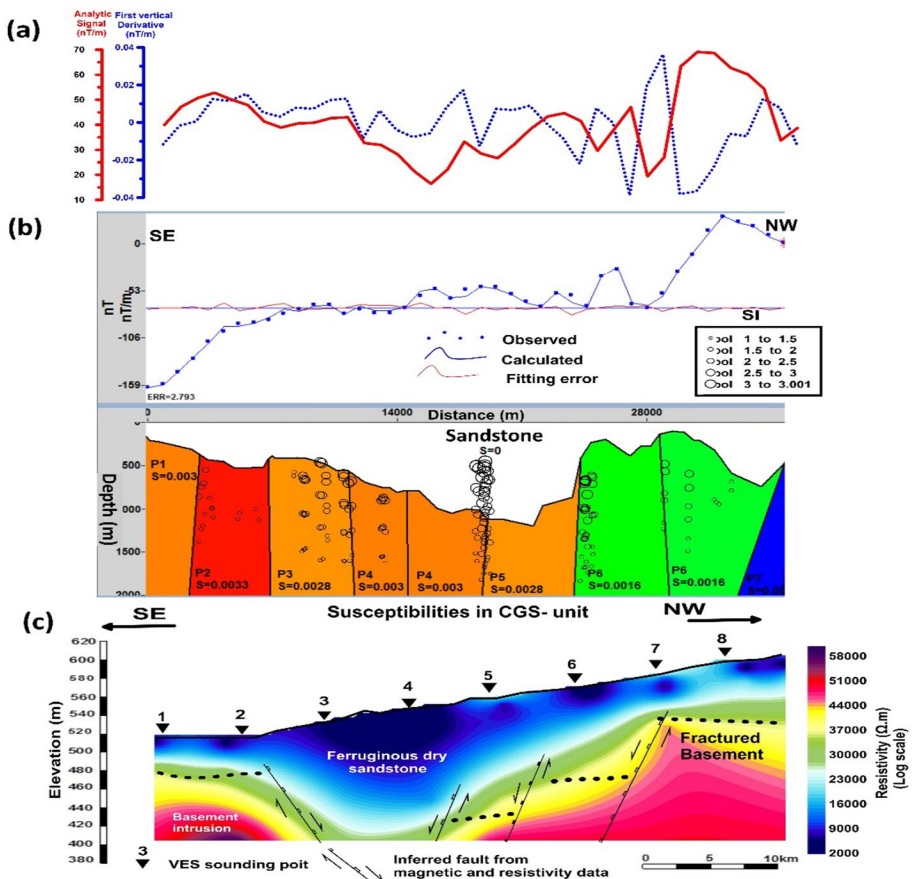


Fig. 17 Integration of land-based magnetic and DC resistivity results at the northwestern side of Gabel Kamel (Eight Bells) **a** graphical plots of the total horizontal derivative and analytical signal, **b** top panel is the modeled RTP magnetic anomaly and bottom panel is 2D magnetic model along with the point source depth solutions of 2D Euler deconvolution, **c** resistivity cross section. For transect location, see Fig. 6a

60 m. The Euler point source depth solutions are superimposed on the magnetic model. The minimum and maximum detectable depths of the major faults are 200 and 1000 m, respectively. According to the constructed magnetic model, the area southeast Eight Bells is structurally suitable for groundwater accumulation. However, from the methodological point of view, the magnetic method cannot only solely be judged on the groundwater potentiality where the extremely high resistivity values (1200–45,000 Ω m) along the profile indicate dry ferruginous sandstone and boulders (Fig. 16c). The variable thickness along the profile could be attributed to the influence of inferred faults. Although the resistivity section and 2D magnetic model clearly depict a basin (Fig. 17b, c), unfortunately, the very high resistivity values (more than 3000 Ω m) suggest the area west of Gabel Kamel ridge to be dry. A possible interpretation is that the basin is closed from the south, in the area between Gabel Uweinat and Gabel Kamel, by basement uplift, which acts as a barrier for the groundwater flow from south to north as deduced from the results of 3D gravity inversion (Fig. 14). To emphasize the role of Uweinat-Gabel Kamel uplift for diminishing the aquifer potentialities, eight resistivity soundings were carried out at Gabel Kamel and Nosb Elamir, and it indicates that the sedimentary cover in these regions is thin and dry based on the inconsistent high resistivity values (> 5000 Ω m) in all sounding points. In these regions, the interpreted depths to the basement surface as indicated from land-based measurement vary from 60 to 85 m. This assumption correlates well with the previous regional-scale results from satellite gravity of the EIGEN-6C4 dataset.

In contrast, the resistivity characteristics in the northeast Gabel Kamel (Fig. 6b) differ significantly from those on the western side of Gabel Kamel ridge, where the resistivity values are intensely decreased to their minimum values in the area (Fig. 18c). As a result, the drop in resistivity values (70–200 Ω m) is attributed to the presence of saturated sands with thickness ranging from 100 to 250 m. In the EW profile (Fig. 18), the analysis of the magnetic derivatives in the western end reveals a shallow basement intrusion with sharp vertical contact due to the impact of Gabel Kamel ridge (NNE) as indicated from the structural map and 3D gravity inversion (Figs. 14, 15). In addition, there is a good match between magnetic and resistivity results at that place where the depth to basement surface is about 20 m with an exceedingly increase in resistivity value (> 5000 Ω m) due to shallow basement intrusion (VES1, Fig. 18c). The most significant observation is that the eastern region is clearly joined with the south and southeast aquifer to increase the suitability of the sandstone overburden for groundwater accumulations as indicated from the perpendicular NS profile (Fig. 19). Moreover, the integration of resistivity and magnetic models along the NS profile displays that this profile runs along a typical NS sub-basin alternating with Gabel Kamel ridge, as indicated from the uniform thickness of sandstone aquifer and great sedimentary cover (> 500 m thick), and confirm the results of TDR and EHGA derivatives and 3D gravity inversions (Figs. 11, 12, 14 respectively). The minimum depth to the basement surface of about 200 m is estimated in the southern end of the NS profile (Fig. 19b). This depth is sufficient for passing the groundwater in the south–north pathway to recharge the aquifer in the north and northeast regions. Therefore, the interpretation of multi-scale geophysical datasets in this hyper-region indicates that the area northeastern Gabel Kamel to GPC-7 well is preferable for drilling new exploratory wells (Fig. 16). This favorable area is considered as the extension of east Uweinat wells and may have considerable high groundwater potentials with freshwater quality (500–1000 ppm).

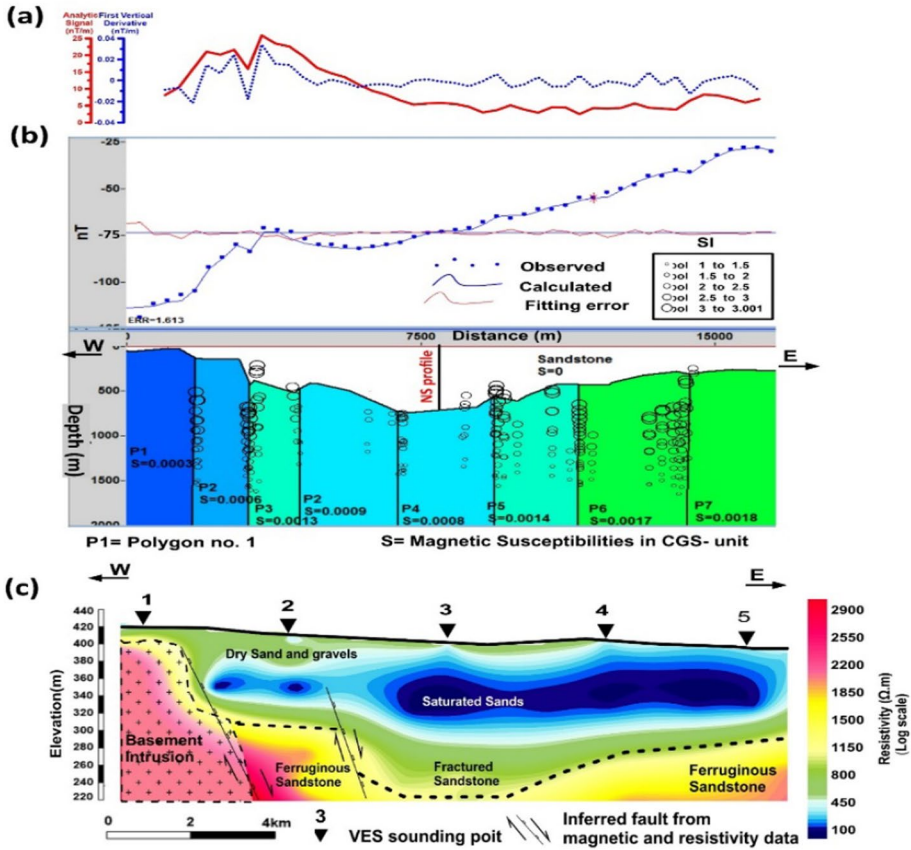


Fig. 18 Integration of land-based magnetic and DC resistivity results along E–W profile at the northeastern side of Gabel Kamel. **a** Graphical plots of the total horizontal derivative and analytical signal, **b** top panel is the modeled RTP magnetic anomaly and bottom panel is 2D magnetic model along with the point source depth solutions of 2D Euler deconvolution, **c** resistivity cross section. For location, see Fig. 6b

3 Summary and Conclusions

The groundwater exploration in arid and hyper-arid regions all over the world is always a challenge due to the lack of hydrogeological information and the poor understanding of the groundwater flow patterns. In this study, an integrated exploration strategy (space-borne gravity and land-based geophysics) was applied to determine the structural control on groundwater potentialities in the southwestern corner of the Egyptian Western Desert as a typical example of a hyper-arid environment.

For regional mapping, the various mathematical derivatives of the EIGEN-6C4 model as TAD and EHGA can be effectively used for better understanding the structural framework that may control the groundwater flow and subsequently the promising sites for the groundwater accumulation with large scale in arid regions. The hybrid gravity models like the EIGEN-6C4 gravity model can be used for regional mapping of mega-structures in inaccessible areas where ground geophysical surveys are difficult to conduct to cover the entire area. The results from the satellite gravity data, land-magnetic and resistivity surveys

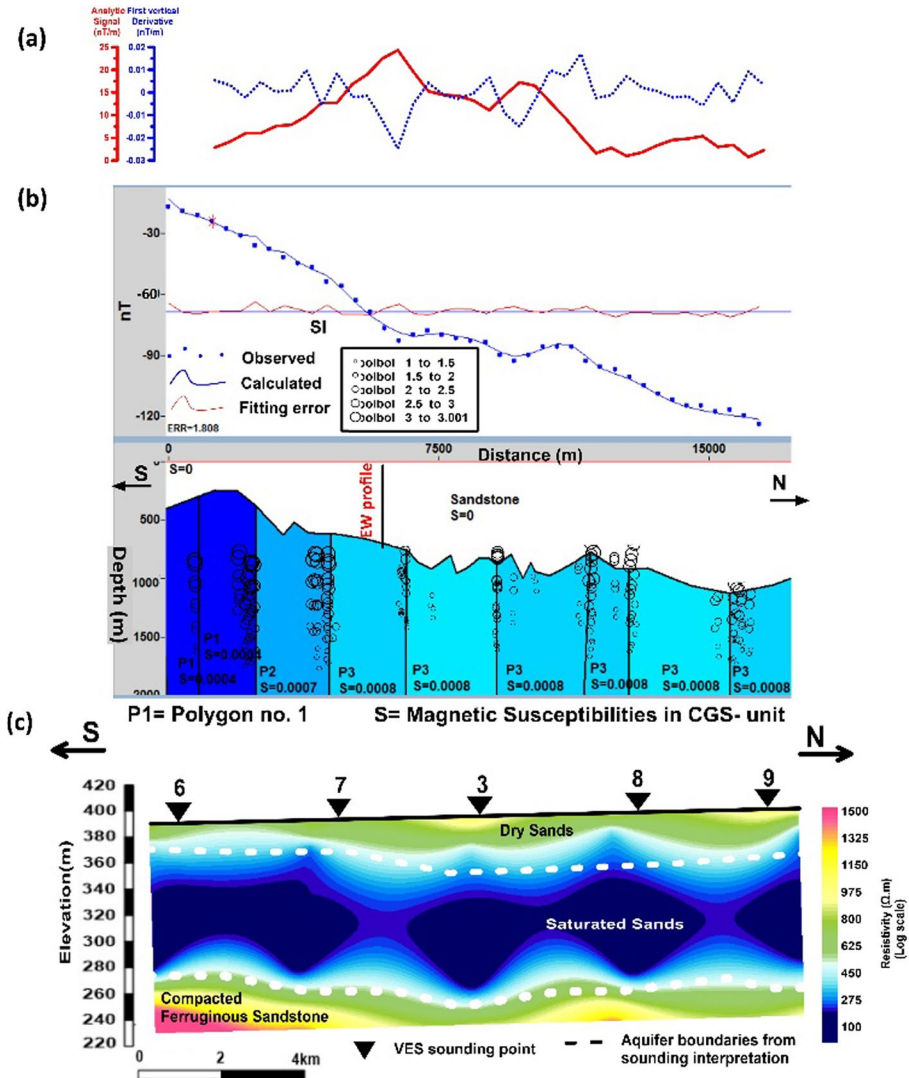


Fig. 19 Integration of land-based magnetic and DC resistivity results along N–S profile at the northeastern side of Gabel Kamel. **a** Graphical plots of the total horizontal derivative and analytical signal, **b** top panel is the modeled RTP magnetic anomaly and bottom panel is 2D magnetic model along with the point source depth solutions of 2D Euler deconvolution, **c** geoelectric cross section. For transect location, see Fig. 6b

were compared and validated with foregoing regional geological, hydrogeology obtained from remote sensing and boreholes data. These results demonstrate the effectiveness of global satellite-derived gravity data in the study of geologically interesting areas, while the integration of magnetic and DC resistivity methods approves their capabilities as useful tools for groundwater exploration in hyper-arid environments. The applied integrative procedure demonstrates the importance of multi-scale geophysical investigations, to assist in water resource management decisions and support the much-needed agricultural expansion

in the extremely arid regions. The adopted methodology can be applied in a similar way to other areas elsewhere with appropriate modifications for identifying candidate well locations. However, satellite datasets could not identify geological features at a finer scale as a direct groundwater exploration tool. In this case, it can act as a preliminary stage for planning high-resolution investigations using DC impedance and geomagnetic surveys. Hence, this study displays how integrating multi-source datasets as a time and cost-effective tool is critical to sound groundwater exploration under structurally controlled conditions as in the case of the Egyptian Western Desert.

In the area of Gabel Kamel, the southwestern corner of the Egyptian Western Desert, the trend analyses show that the dominant tectonic trends are E–W and N–S in the western side from the area and NNE–SSW and NE–SW trends in the east. These structures play an important role in controlling the aquifer depths and recharge system where the E–W igneous intrusions and shallow basement blocks in the west act as barriers in the direction of water flow from the south or from the west during the wet period in the Early Holocene. Therefore, the current results will be shared with the local government and decision-makers to conserve the sustainability of the aquifer system in the east of the Uweinat area and design a long-term management plan for optimum use of the groundwater resource in this hyper-arid region.

In future work plans and based on the current results, additional exploratory wells should be drilled in the area east and northeast of Gabel Kamel for water sampling and isotope studies for better understanding the origin and groundwater flow trends related to the inferred subsurface structures. More detailed DC resistivity surveys may be required in this region to delineate the accurate depth and thickness of the saturated zone for boreholes siting. Further, the aquifer characterization and transport models could be estimated by considering the NE–SW and E–W faults as preferential flow paths. An updated numerical model should be constructed to improve the water resources management strategy that will allow us to better understand more realistic scenarios by considering the recharging system and groundwater movement in the area. To simulate the groundwater flow, the appropriate aquifer parameters could be used from the geophysical logs and pumping tests.

Acknowledgements The authors gratefully acknowledge the International Centre for Global Earth Models (ICGEM) for providing EIGEN-6C4 gravity data, as well as Scripps Institution of Oceanography, University of California San Diego USA for providing TOPEX-1min gravity data for free. The authors would also like to express their gratitude to the National Water Research Center (NWRC) and the Research Institute for Groundwater (RIGW) for their assistance in accomplishing the field work.

References

- Abdel Hafeeza ThH, Sabeta HS, El-Sayedb AN, Zayeda MA (2018) Geoelectrical exploration of groundwater at West Dayrout Area, Assiut Governorate, Egypt. *NRIAG J Astron Geophys* 7(2):279–296. <https://doi.org/10.1016/j.nrjag.2018.07.004>
- Abdelkareem M, El-Baz F (2015) Evidence of drainage reversal in the NE Sahara revealed by space-borne remote sensing data. *J Afr Earth Sci* 110:245–257. <https://doi.org/10.1016/j.jafrearsci.2015.06.019>
- Abdelkareem M, El-Baz F (2017) Remote sensing of paleodrainage systems west of the Nile River, Egypt. *Geocarto Int* 32(5):541–555. <https://doi.org/10.1080/10106049.2016.1161076>
- Abdul Fattah R, Meekees JAC, Colella S, Bouman J, Schmidt M, Ebbing J (2013). The application of GOCE satellite gravity data for basin and petroleum system modeling: a case-study from the Arabian Peninsula; Search and Discovery Article #120130 (2013), Posted March 13, 2013. Adapted from extended abstract prepared in conjunction with poster presentation at AAPG Hedberg Conference, Petroleum Systems: Modeling The Past, Planning The Future, 1–5 October 2012, Nice, France, AAPG©2012

- Ahmed M, Sultan M, Wahr J, Yan E (2014) The use of GRACE data to monitor natural and anthropogenic induced variations in water availability across Africa. *Earth Sci Rev* 136(289–300):2014. <https://doi.org/10.1016/j.earscirev.2014.05.009>
- Alabi AA, Bello R, Ogungbe AS, Oyerinde HO (2010) Determination of ground water potential in Lagos State University, Ojo; using geoelectric methods (vertical electrical sounding and horizontal profiling). *Rep Opin* 2(5):68–75
- Andersen OB, Knudsen P, Berry PAM (2009) The DNSC-08GRA global marine gravity field from double retracked satellite altimetry. *J Geod* 84(3):191–199. <https://doi.org/10.1007/s00190-009-0355-9>
- Anomohanran O (2011) Determination of groundwater potential in Asaba, Nigeria using surface geoelectric sounding. *Int J Phys Sci* 6(33):7651–7656. <https://doi.org/10.5897/IJPS11.1549>
- Apollinaire B, Joseph K, Tabod TC, Loudi Y, Robert N, Ludovic KH, Valentin O (2017) Subsurface structural mapping using combined terrestrial and grace gravity data of the Adamawa plateau (North-Camereroon). *Int J Geosci* 8:869–887. <https://doi.org/10.4236/ijg.2017.87050>
- Bello HI, Alhassan UD, Salako KA, Rafiu AA, Adetona AA, Shehu J (2019) Geoelectrical investigation of groundwater potential, at Nigerian Union of Teachers Housing estate, Paggo, Minna, Nigeria. *Appl Water Sci* 9:52. <https://doi.org/10.1007/s13201-019-0922-z>
- Block AE, Bell RE, Studinger M (2009) Antarctic crustal thickness from satellite gravity: implications for the Transantarctic and Gamburtsev Subglacial Mountains. *Earth Planet Sci Lett* 288:194–203. <https://doi.org/10.1016/j.epsl.2009.09.022>
- Bobachev A, Modin I, Shevinin V (2008) IPI2Win V2.0: user's guide. Moscow State University, Moscow. <http://geophys.geol.msu.ru/ipi2win.htm>
- Bomfim EP, Braitenberg C, Molina EC (2013) Mutual evaluation of global gravity models (EGM2008 and GOCE) and terrestrial data in Amazon Basin, Brazil. *Geophys J Int* 195(2):870–882. <https://doi.org/10.1093/gji/ggt283>
- Braitenberg C, Ebbing J (2009) New insights into the basement structure of the West-Siberian basin from forward and inverse modelling of GRACE satellite gravity data. *J Geophys Res* 114:Bo6402. <https://doi.org/10.1029/2008JB005799>
- Braitenberg C, Mariani P, Ebbing J, Sprlak M (2011) The enigmatic Chad lineament revisited with global gravity and gravity-gradient fields. *Geol Soc Lond Spec Publ* 357:329–341
- Brügge N (2017) Remarks to the geological origin of the hills "Eight Bells" at the southern Gilf Kebir (Egypt). http://www.b14643.de/Sahara/Eight_Bells/index.htm. Last update 10 May 2017
- Bubener O, Embabi NS, Ashour MM (2020) Sand seas and dune fields of Egypt. *Geosciences* 10:101. <https://doi.org/10.3390/geosciences10030101>
- Chouhan AK, Choudhury P, Pal SK (2020) New evidence for a thin crust and magmatic underplating beneath the Cambay rift basin, Western India through modelling of EIGEN-6C4 gravity data. *J Earth Syst Sci* 129:64. <https://doi.org/10.1007/s12040-019-1335-y>
- Ebraheem A, Riad S, Wycisk P, Seif ElNasr A (2003) Simulation of impact of present and future groundwater extraction from the non-replenished Nubian Sandstone Aquifer in southwest Egypt. *Environ Geol* 43:188–196. <https://doi.org/10.1007/s00254-002-0643-7>
- Ekinci YL, Ertekin C, Yiğitbaş E (2013) On the effectiveness of directional derivative based filters on gravity anomalies for source edge approximation: synthetic simulations and a case study from the Aegean graben system (western Anatolia, Turkey). *J Geophys Eng* 10(3):035005. <https://doi.org/10.1088/1742-2132/10/3/035005>
- Ekka MS, Debasis MS, Sahoo R, Pal K, Roy PNS, Mishra OP (2022) Comparative analysis of the structural pattern over the Indian Ocean basins using EIGEN6C4 Bouguer gravity data. *Geocarto Int*. <https://doi.org/10.1080/10106049.2022.2087748>
- El Alfy M (2014) Numerical groundwater modelling as an effective tool for management of water resources in arid areas. *Hydrol Sci J* 59(6):1259–1274. <https://doi.org/10.1080/02626667.2013.836278>
- El Shinawi A, Ramadan F, Zelenakova M (2021) Appraisal for the environment, weathering and provenance of Upper Cretaceous Lower Tertiary shales, Western Desert, Egypt. *Acta Montan Slovaca* 26(1):171–184
- El-Baz F (1998) Sand accumulation and groundwater in the Eastern Sahara. *Episodes* 21(3):147–151. <https://doi.org/10.18814/epiugs/1998/v21i3/002>
- El-Baz F (2000) Satellite observations of the interplay between wind and water processes in the Great Sahara. *Photogram Eng Remote Sens* 66(6):777–782
- El-Baz F (1995) Utilizing satellite images for ground water exploration in fracture zone aquifers. In: Proceedings of international conference on water resources management in arid countries, Muscat Oman, vol 2, pp 419–427
- Elewa HH, Ramadan EM, Nosair AM (2016) Spatial-based hydro-morphometric watershed modeling for the assessment of flooding potentialities. *Environ Earth Sci*. <https://doi.org/10.1007/s12665-016-5692-4>

- Elewa HH, Zelenakova M, Nosair AM (2021) Integration of the analytical hierarchy process and gis spatial distribution model to determine the possibility of runoff water harvesting in dry regions: Wadi Watir in Sinai as a case study. *Water* 13(6):804. <https://doi.org/10.3390/w13060804>
- El-Ghawabi M (1987) Use of Landsat-images for interpretation of the geologic evolution of the Gilf Kebir area, SW Egypt. In: Proceedings of international workshop on remote sensing and resource exploration. ICTP, Trieste, Italy
- El-Meselhy A, Abdelhalim A, Bassem SN (2020) Geospatial analysis in groundwater resources management as a tool for reclamation areas of New Valley (El-Oweinat). *Egypt J Afr Earth Sci* 162:103720
- Famiglietti J (2014) The global groundwater crisis. *Nat Clim Change* 4:945–948. <https://doi.org/10.1038/nclimate2425>
- Förste C, Bruinsma SL, Abrykosov O, Lemoine J, Marty JC, Flechtner F, Balmino G, Barthelmes F, Biancale R (2014) EIGEN-6C4 The latest combined global gravity field model including GOCE data up to degree and order 2190 of GFZ Potsdam and GRGS Toulouse. *GFZ Data Serv.* <https://doi.org/10.5880/icgem.2015.1>
- Foster SSD, Chilton PJ (2004) Groundwater: the processes and global significance of aquifer degradation. *Philos Trans R Soc Lond B* 2003(358):1957–1972. <https://doi.org/10.1098/rstb.2003.1380>
- Foster S, Loucks D (2006) Non-renewable groundwater resources. *UNESCO IHP-VI Ser Groundw* 10:81
- Gaber A, Koch M, Helmi M, Sato M (2011) SAR remote sensing of buried faults: implications for groundwater exploration in the Western Desert of Egypt. *Sens Imaging* 12(3/4):133–151. <https://doi.org/10.1007/s11220-011-0066-1>
- Gambetta M, Armadillo E, Carmisciano C, Caratori Tontini F, Bozzo E (2007) Magnetic Base Station Deceptions, a magnetovariational analysis along the Ligurian Sea coast, Italy. *Ann Geophys* 50(3):397–406. <https://doi.org/10.4401/ag-4423>
- Gaulier JM, Le Pichon X, Lyberis N, Avedik F, Geli L, Moretti I, Deschamps A, Hafez S (1988) Seismic study of the crust of the northern Red Sea and Gulf of Suez. *Tectonophysics* 153:55–88. [https://doi.org/10.1016/0040-1951\(88\)90007-8](https://doi.org/10.1016/0040-1951(88)90007-8)
- Gemail Kh (2015) Application of 2D resistivity profiling for mapping and interpretation of geology in a till aquitard near Luck Lake, Southern Saskatchewan, Canada. *Environ Earth Sci* 73:923–935. <https://doi.org/10.1007/s12665-014-3441-0>
- Gemail Kh, Abd-El Rahman NM, Ghiath BM, Aziz RN (2016) Integration of ASTER and airborne geophysical data for mineral exploration and environmental mapping: a case study, Gabal Dara, North Eastern Desert, Egypt. *Environ Earth Sci* 75:592. <https://doi.org/10.1007/s12665-016-5368-0>
- Gemail Kh, Atwa M, Elarky M, Zamzam S (2017) Imaging of wastewater percolation in heterogeneous soil using electrical resistivity tomography (ERT): a case study at east of Tenth of Ramadan City, Egypt. *Environ Earth Sci* 76(11):2018–2021
- Gemail K, Ibrahim A, Bedair S (2021a) Geophysical groundwater exploration in arid regions using integrated land-based magnetic and DC resistivity measurements: a case study at Gilf Kebir area, South Western Desert, Egypt. In: Negm A, Elkhoully A (eds) *Groundwater in Egypt's deserts*. Springer water. Springer, Cham. https://doi.org/10.1007/978-3-030-77622-0_5
- Gemail K, Masoud AA, Elhoriny MM, Atwia MG, Katsuaki K (2021b) Hydrogeophysical investigations using DC resistivity survey to assess the water potentialities of the shallow aquifer zone in East of Dakhla Oasis, Egypt. In: *Sustainable water solutions in the Western Desert, Egypt: Dakhla Oasis*. https://doi.org/10.1007/978-3-030-64005-7_15
- Ghoneim E (2011) Ancient mega rivers, inland deltas and lake basins of the Eastern Sahara: a radar remote sensing investigation. *Geol Soc Am Abs Programs* 43(5):141
- Ghoneim E, El-Baz F (2007) The application of radar topographic data to mapping of a mega-paleodrainage in the Eastern Sahara. *J Arid Environ* 69(4):658–675. <https://doi.org/10.1016/j.jaridenv.2006.11.018>
- Ghoneim E, Robinson C, El-Baz F (2007) Radar topography data reveal drainage relics in the eastern Sahara. *Int J Remote Sens* 28(8):1759–1772. <https://doi.org/10.1080/01431160600639727>
- Ghoneim E, El-Baz F (2020) Satellite image data integration for groundwater exploration in Egypt. In: Elbeih R et al (eds) *Environmental remote sensing in Egypt*. Springer, New York. <https://doi.org/10.1007/978-3-030-39593-3>
- Ghoneim E, El-Baz F (2008) Mapping water basins in the Eastern Sahara by SRTM data. In: *IEEE international geoscience and remote sensing symposium, vol 1, 6–11 July, Boston, Massachusetts, USA*, pp 1–4. <https://doi.org/10.1109/IGARSS.2008.4778777>
- Gómez-Alday JJ, Hussein S, Arman H, Alshamsi D, Murad A, Elhaj K, Aldahan A (2022) Multi-isotopic evaluation of groundwater in a rapidly developing area and implications for water management in

- hyper-arid regions. *Sci Total Environ* 805, Article 150245. <https://doi.org/10.1016/j.scitotenv.2021.150245>
- Gouet DH, Meying A, Nkougou HLE, Assembe SP, Nouck PN, Mbarga TN (2020) Typology of sounding curves and lithological 1D models of mineral prospecting and groundwater survey within crystalline basement rocks in the east of Cameroon (Central Africa) using electrical resistivity method and Koeffoed computation method. *Hindawi Int J Geophys*. <https://doi.org/10.1155/2020/8630406>
- Grolier M, Schultejeann P (1982) Geology of the southern Gilf Kebir plateau and vicinity, Western Desert, Egypt. In: El-Baz F, Maxwell T (eds) *Desert landforms of Southwest Egypt: a basis for comparison with Mars*. NASA, Washington, pp 189–206
- Hassan S, Sultan M, Sobh M, Elhebery MS, Zahran K, Abdeldayem A, Issawy E, Kamh S (2021) Crustal structure of the Nile delta: interpretation of seismic-constrained satellite-based gravity data. *Remote Sens* 13:1934. <https://doi.org/10.3390/rs13101934>
- Herrera C, Godfrey L, Urrutia J, Custodio E, Jordan T, Jódar J, Delgado K (2021) Recharge and residence times of groundwater in hyper arid areas: the confined aquifer of Calama, Loa River Basin, Atacama Desert. *Chile Sci Total Environ* 15, Article 141847
- Hesse K-H, Hissene A, Kheir O, Schnaecker E, Schneider M, Thorweihe U (1987) Hydrogeological investigations of the Nubian Aquifer System, Eastern Sahara. *Berl Geowiss Abh Ser A* 75:397–464
- Huang F, Zhang YD, Zhang DR, Chen X (2019) Environmental groundwater depth for groundwater-dependent terrestrial ecosystems in arid/semiarid regions: a review. *Int J Environ Res Public Health* 16:763. <https://doi.org/10.3390/ijerph16050763>
- Ince ES, Barthelmes F, Reißbald S, Elger K, Förste C, Flechtner F, Schuh H (2019) ICGEM-15 years of successful collection and distribution of global gravitational models, associated services and future plans. *Earth Syst Sci Data* 11:647–674. <https://doi.org/10.5194/essd-11-647-2019>
- Iserhien-Emekeme RE, Atakpo EA, Emekeme OL, Anomohanran O (2004) Geoelectric survey for groundwater in AgbedeEtsako West L.G.A., Edo State. *Adv Nat Appl Sci Res* 2(1):65–72
- Issawi B (1978) New findings on the geology of Uweinat-Gilf Kebir. *Ann Geol Surv Egypt* 8:27–293
- Issawi B, Jux U (1982) Contribution to the stratigraphy of the Paleozoic rocks in Egypt. *Geol Surv Egypt* 64:1–24
- Issawi B, Sallam E (2018) Stratigraphy and facies development of the pre-Cenozoic sediments in southern Egypt: a geodynamic approach. *Arab J Geosci* 11:271. <https://doi.org/10.1007/s12517-018-3626-z>
- Kamerman P (2020) Using raster data to calculate and then map aridity indices. <https://www.painblogr.org/2020-12-15-climate-change>. Accessed 15 Dec 2020
- Khiabani MY, Mehdy S, Shahdany H, Hassani Y, Maestre JM (2021) Introducing an economic agricultural water distribution in a hyper-arid region: a case study in Iran. *J Hydroinform* 23(3):548–566. <https://doi.org/10.2166/hydro.2021.008>
- Kuper R, Kröpelin S (2006) Climate-controlled Holocene occupation in the Sahara: motor of Africa's evolution. *Science* 313:803–807. <https://doi.org/10.1126/science.1130989>
- Laake A (2011) Integration of satellite imagery, geology and geophysical data, earth and environmental sciences. In: Dar IA, Dar MA (eds) *IntechOpen*. <https://doi.org/10.5772/27613>. <https://www.intechopen.com/books/earth-and-environmental-sciences/integration-of-satellite-imagery-geology-and-geophysical-data>
- Landerer FW, Swenson SC (2012) Accuracy of scaled GRACE terrestrial water storage estimates. *Water Resour Res* 48:W04531. <https://doi.org/10.1029/2011WR011453>
- Li Y, Oldenburg DW (1996) 3D inversion of magnetic data. *Geophysics* 61(2):394–408. <https://doi.org/10.1190/1.1443968>
- Li C, Zhou Z, Li J, Chen H, Geng J, Li H (2007) Precollisional tectonics and terrain amalgamation offshore southern Taiwan: characterizations from reflection seismic and potential field data. *Sci China Ser D* 50:897–908. <https://doi.org/10.1007/s11430-007-0025-9>
- Linstädter J (2007) Rocky islands within oceans of sand—archaeology of the Jebel Ouenat/Gilf Kebir region, Eastern Sahara. In: Bubenzer, O., Bolten, A., F. Darius (eds.) *Atlas of environmental and cultural change in arid Africa*. *Afr Praehist* 21:34–37
- Linstädter J, Stefan Kröpelin S (2004) Wadi Bakht revisited: Holocene climate change and prehistoric occupation in the Gilf Kebir region of the Eastern Sahara, SW Egypt. *Geoarchaeology* 19(8):753–778. <https://doi.org/10.1002/gea.20023>
- Mahmoud HH, Kotb AD (2017) Impact of the geological structures on the groundwater potential using geophysical techniques in West Bani Mazar Area, El Minia-Western Desert, Egypt. *J Afr Earth Sci* 130:161–173. <https://doi.org/10.1016/j.jafrearsci.2017.03.024>

- Mansour N (1991) Redepositions and structural development of the Uweinat-Safsaf-Aswan uplift system. *J Afr Earth Sci Middle East*. [https://doi.org/10.1016/0899-5362\(91\)90019-U](https://doi.org/10.1016/0899-5362(91)90019-U)
- Marsouk IA (1988) Study of crustal structure of Egypt deduced from deep seismic and gravity data. Ph.D. dissertation, Hamburg, Germany, Hamburg University
- Masoud AA, El-Horiny MM, Atwia MG, Gemail K, Koike K (2018) Assessment of groundwater and soil quality degradation using multivariate and geostatistical analyses, Dakhla Oasis, Egypt. *J Afr Earth Sci* 142:64–81. <https://doi.org/10.1016/j.jafrearsci.2018.03.009>
- Masoud AA, El-Horiny MM, Atwia MG, Koike KG, K (2019) Mapping soil salinity using spectral mixture analysis of landsat 8 OLI images to identify factors influencing salinization in an arid region. *Int J Appl Earth Observ Geoinform* 83(2019):101944. <https://doi.org/10.1016/j.jag.2019.101944>
- McCaughey JF, Breed C, Schaber GG, Haynes CV, Issawi B, El-Kilani A (1986) Palaeodrainages of the Eastern Sahara. The Radar River revisited (SIR-A/B implications for a Mid-Tertiary Trans-African Drainage System). *IEEE Trans Geo Sci Remote Sens* 24:624–648
- Meier P et al (2014) Hydrogeophysical investigations in the western and north-central Okavango Delta (Botswana) based on helicopter and ground-based transient electromagnetic data and electrical resistance tomography. *Geophysics* 79(5):B201–B211
- Melati MD, Fleischmann AS, Fan FM, Paiva RC, Athayde G (2019) Estimates of groundwater depletion under extreme drought in the Brazilian semi-arid region using GRACE satellite data: application for a small-scale aquifer. *Hydrogeol J* 27:2789–2802. <https://doi.org/10.1007/s10040-019-02065-1>
- Meneisy M (1990) Volcanicity. In: Said R (ed) *The geology of Egypt*. Balkema, Rotterdam, pp 157–172
- Miller HG, Singh V (1994) Potential field tilt- a new concept for location of potential field sources. *J Appl Geophys* 32(2–3):213–217. [https://doi.org/10.1016/0926-9851\(94\)90022-1](https://doi.org/10.1016/0926-9851(94)90022-1)
- Mohamed A, Sultan M, Ahmed M, Yan E, Ahmed E (2016) Aquifer recharge, depletion, and connectivity: inferences from GRACE, land surface models, and geochemical and geophysical data. *Geol Soc Am Bull* 129(5/6):534–546. <https://doi.org/10.1130/B31460.1>
- Mohamed A, Ahmed E, Alshehri F, Abdelrady A (2022) The groundwater flow behavior and the recharge in the Nubian sandstone aquifer system during the wet and arid periods. *Sustainability* 14:6823. <https://doi.org/10.3390/su14116823>
- Oasis Montaj (2015) Geosoft mapping and application system version 8.3.3, Inc, Suite 500, Richmond St. West Toronto, ON Canada N5S1V6
- Muchingami A, Mkali A, Vinqi L et al (2021) Integration of hydrogeophysical and geological investigations in enhancing groundwater potential assessment in Houtriver gneiss crystalline basement formation of South Africa. *Phys Chem Earth a/b/c* 123:103009
- Nabawy Bassem S, Rochette P, Géraud Y (2009) Petrophysical and magnetic pore network anisotropy of some cretaceous sandstone from Tushka Basin, Egypt. *Geophys J Int* 177(1):43–61. <https://doi.org/10.1111/j.1365-246X.2008.04061.x>
- Nabawy Bassem S, Rochette P, Géraud Y (2010) Electric pore fabric of the Nubia sandstones in south Egypt: characterization and modelling. *Geophys J Int* 183(2):681–694. <https://doi.org/10.1111/j.1365-246X.2010.04789.x>
- Narayan S, Sahoo SD, Pal SK, Kumar U, Pathak VK, Majumdar TJ, Chouhan A (2017) Delineation of structural features over a part of the Bay of Bengal using total and balanced horizontal derivative techniques. *Geocarto Int* 32(4):351–366. <https://doi.org/10.1080/10106049.2016.1140823>
- Obenson G (1974) A 1973 gravimetric geoid of Africa. *Geophys J Int* 37:271–283. <https://doi.org/10.1111/j.1365-246X.1974.tb01238.x>
- Oldenborger GA, Pugin AJ-M, Pullan SE (2013) Airborne time-domain electromagnetics, electrical resistivity and seismic reflection for regional three-dimensional mapping and characterization of the Spiritwood Valley Aquifer, Manitoba, Canada. *Near Surf Geophys* 11(1):63–74. <https://doi.org/10.3997/1873-0604.2012023>
- Oruc B (2010) Edge detection and depth estimation using a tilt angle map from gravity gradient data of the Kozaklı-Central Anatolia region, Turkey. *Pure Appl Geophys* 168(10):1769–1780. <https://doi.org/10.1007/s00024-010-0211-0>
- Oruc B, Keskinsezer A (2008) Structural setting of the Northeastern Biga Peninsula (Turkey) from tilt derivatives of gravity gradient tensors and magnitude of horizontal gravity components. *Pure Appl Geophys* 165(9):1913–1927. <https://doi.org/10.1007/s00024-008-0407-8>
- Parsekian AD, Singha K, Minsley BJ, Holbrook WS, Slater L (2015) Multiscale geophysical imaging of the critical zone. *Rev Geophys*. <https://doi.org/10.1002/2014RG000465>
- Pham LT, Eldosouky AM, Oksum E, Saada SA (2020) A new high resolution filter for source edge detection of potential field data. *Geocarto Int*. <https://doi.org/10.1080/10106049.2020.1849414>
- Rabeh T, Bedair S, Abdel-Zaher M (2018) Structural control of hydrogeological aquifers in the Bahariya Oasis, Western Desert, Egypt. *Geosci J* 22:145–154. <https://doi.org/10.1007/s12303-016-0072-3>


- Reid AB, Allsop JM, Granser H, Millett AJ, Somerton IW, Reid AB, Allsop JM, Granser HA, Millett J, Somerton IW (1990) Magnetic interpretation in three dimensions using Euler deconvolution. *Geophysics* 55(1):80–91. <https://doi.org/10.1190/1.1442774>
- Robinson CA (2002) Application of satellite radar data suggest that the Kharga Depression in southwestern Egypt is a fracture rock aquifer. *Int J Remote Sens* 23(19):4101–4113. <https://doi.org/10.1080/01431160110115933>
- Robinson CA, El-Baz F, Singhroy V (1999) Subsurface imaging by Radarsat: comparison with Landsat TM data and implications to ground water in the Selima area, North-western Sudan. *Can J Remote Sens* 25:268–277. <https://doi.org/10.1080/07038992.1999.10874725>
- Robinson CA, El-Baz F, Ozdogan M, Ledwith M, Blanco D, Oakley S, Inzana J (2000) Use of radar data to delineate palaeodrainage flow directions in the Selima Sand Sheet, Eastern Sahara. *Photogramm Eng Remote Sens* 66:745–753
- Robinson CA, Werwer A, El-Baz F et al (2007) The Nubian aquifer in Southwest Egypt. *Hydrogeol J* 15:33–45. <https://doi.org/10.1007/s10040-006-0091-7>
- Robinson C, El-Kaliouby H, Ghoneim E (2017) Influence of structures on drainage patterns in the Tushka Region, SW Egypt. *J Afr Earth Sci (spec Issue)* 136:262–271. <https://doi.org/10.1016/j.jafrearsci.2017.01.004>
- Rodell M, Chen J, Kato H, Famiglietti J, Nigro J, Wilson C (2007) Estimating ground water storage changes in the Mississippi River basin (USA) using GRACE. *Hydrogeol J* 15(1):159–166. <https://doi.org/10.1007/s10040-006-0103-7>
- Rodell M, Velicogna I, Famiglietti JS (2009) Satellite-based estimates of groundwater depletion in India. *Nature* 462:999–1002. <https://doi.org/10.1038/nature08238>
- Rune Floberghagen R, Fehring M, Lamarre D et al (2020) Erratum to: Mission design, operation and exploitation of the Gravity field and steady-state Ocean Circulation Explorer (GOCE) mission. *Bull Gæodésique* 85(11):749–758. <https://doi.org/10.1007/s00190-012-0541-z>
- Sahour HR, Sultan M, Abdellatif B, Emil M, Abotalib ZA, Abdelmohsen K, Vazifedan M, Mohammad AT, Hassan SM, Metwalli MR, El Bastawesy M (2022) Identification of shallow groundwater in arid lands using multi-sensor remote sensing data and machine learning algorithms. *J Hydrol* 614:128509. <https://doi.org/10.1016/j.jhydrol.2022.128509>
- Saibi H, Hag DB, Alamri MSM, Ali HA (2021) Subsurface structure investigation of the United Arab Emirates using gravity data. *Open Geosci* 13:262–271. <https://doi.org/10.1515/geo-2020-0233>
- Salako KA, Adetona AA, Rafiu AA, Ofor NP, Alhassan UD, Udensi EE (2009) Vertical electrical sounding investigation for ground-water at the southwestern part (site A) of Nigeria Mobile Police barracks (MOPOL 12), David Mark road, Maitumbi, Minna. *J Sci Educ Technol* 2:350–362
- Saleh S, Jahr T, Jentzsch G, Saleh A, Ashour NMA (2006) Crustal evaluation of the northern Red Sea rift and Gulf of Suez, Egypt, from geophysical data: 3-dimensional modeling. *J Afr Earth Sci* 45:257–278. <https://doi.org/10.1016/j.jafrearsci.2006.02.001>
- Salem AA (2015) Hydrogeological studies on the shallow aquifers in the Area West Samalot El-Minia Governorate, Egypt. *Egypt J Pure Appl Sci* 53(4):49–60. <https://doi.org/10.21608/ejaps.2016.184790>
- Sander P (2006) Lineaments in groundwater exploration: a review of applications and limitations. *Hydrogeol J* 15(1):71–74. <https://doi.org/10.1007/s10040-006-0138-9>
- Sandwell DT, Smith WHF (2009) Global marine gravity from retracked Geosat and ERS-1 altimetry: Ridge Segmentation versus spreading rate. *J Geophys Res* 114:B01411. <https://doi.org/10.1029/2008JB006008>
- Sandwell DT, Garcia E, Soofi K, Wessel P, Smith WHF (2013) Towards 1 mGal global marine gravity from CryoSat-2, Envisat, and Jason-1. *Lead Edge* 32(8):892–899. <https://doi.org/10.1190/tle32.080892.1>
- Sandwell DT, Müller RD, Smith WHF, Garcia E, Francis R (2014) New global marine gravity model from CryoSat-2 and Jason-1 reveals buried tectonic structure. *Science* 346(6205):65–67. <https://doi.org/10.1126/science.1258213>
- Sarvesh K, Pal SK, Guha A, Sahoo SD, Mukherjee A (2022) New insights on Kimberlite emplacement around the Bundelkhand Craton using integrated satellite-based remote sensing, gravity and magnetic data. *Geocarto Int* 37(4):999–1021. <https://doi.org/10.1080/10106049.2020.1756459>
- Senosy MM, Youssef MM, Zaher MA (2013) Sedimentary cover in the south Western Desert of Egypt as deduced from Bouguer gravity and drill-hole data. *J Afr Earth Sci* 82:1–14. <https://doi.org/10.1016/j.jafrearsci.2013.02.001>
- Shacko R, Förste C, Abrikosov O, Bruinsma S, Marty J-C, Lemoine J-M, Dahle C (2013) EIGEN-6C: a high-resolution global gravity combination model including GOCE data. In: *Observation of the*

- system earth from space—CHAMP, GRACE, GOCE and future missions, pp 155–161. https://doi.org/10.1007/978-3-642-32135-1_20
- Simmers I (1997) Recharge of phreatic aquifers in (semi-)arid areas. IAH Int Contrib Hydrogeol 19, AA Balkema, Rotterdam
- Singh A, Raju A (2020) Application of grace satellite data for assessment of groundwater resources in Central Ganga Alluvial Plain, Northern India. In: Shukla V, Kumar N (eds) Environmental concerns and sustainable development. Springer, Singapore. https://doi.org/10.1007/978-981-13-5889-0_7
- Sultan M, Ahmed M, Sturchio N, Yan E, Milewski A, Becker R, Wahr J, Becker D, Chouinard K (2013) Assessment of the Vulnerabilities of the Nubian Sandstone Fossil Aquifer; North Africa. *Clim Vulnerability* 5:311–333
- Sun AY (2013) Predicting groundwater level changes using GRACE data. *Water Resour Res* 49:5900–5912. <https://doi.org/10.1002/wrcr.20421>
- Tapley BD, Kim MC (2000) Chapter 10 applications to geodesy. In: Lee-Lueng F, Anny C (eds) International geophysics. Academic Press, Cambridge
- Th PL, Oliveira SP, Le MH, Trinh PT, Van Tich Vu, Duong V-H, Ngo T-N, Do TD, Nguyen TH, Eldosouky AM (2021) Delineation of structural lineaments of the Southwest Sub-basin (East Vietnam Sea) using global marine gravity model from CryoSat-2 and Jason-1 satellites. *Geocarto Int.* <https://doi.org/10.1080/10106049.2021.1981463>
- Thompson DT (1982) EULDPH: a technique for making computer assisted depth estimates from magnetic data. *Geophysics* 47:31–37. <https://doi.org/10.1190/1.1441278>
- Thorweihe U (1986) Isotopic identification and mass balance of the Nubian Aquifer System in Egypt. In: Thorweihe U (ed) Impact of climatic variations on East Saharian groundwater—modelling of large scale flow regimes, proceedings of a workshop on hydrology. Berlin, Berliner Geowissenschaftliche Abhandlungen, series A, vol 72, pp 87–97
- Tiwari VM, Wahr JM, Swenson S (2009) Dwindling groundwater resources in northern India, from satellite gravity observations. *Geophys Res Lett* 36:L18401. <https://doi.org/10.1029/2009GL039401>
- Toushmalani R, Saibi H (2015a) Fast 3D inversion of gravity data using Lanczos bidiagonalization method. *Arab J Geosci* 8:4969–4981. <https://doi.org/10.1016/j.jappgeo.2016.07.013>
- Toushmalani R, Saibi H (2015b) 3D gravity inversion using Tikhonov regularization. *Acta Geophys* 63(4):1044–1065. <https://doi.org/10.1515/acgeo-2015-0029>
- USGS (2002) Map showing geology, oil and gas fields and geological provinces of Africa. U.S. Geological Survey: Open File Report 97-470A, version 2.0. <http://pubs.usgs.gov/of/1997/ofr-97-470/OF97-470A/>. Accessed July 2013
- Vaish J, Pal SK (2015) Geological mapping of Jharia Coalfield, India using GRACE EGM2008 gravity data: a vertical derivative approach. *Geocarto Int* 30(4):388–401. <https://doi.org/10.1080/10106049.2014.905637>
- Vedanti N, Srivastava RP, Sagode J, Dimri VP (2005) An efficient 1D OCCAM'S inversion algorithm using analytically computed first-and second-order derivatives for the resistivity soundings. *Comput Geosci* 31:319–328
- Verduzco B, Fairhead JD, Green CM, MacKenzie C (2004) New insights into magnetic derivatives for structural mapping. *Lead Edge* 23:116–119. <https://doi.org/10.1190/1.1651454>
- Wrathall DJ, Hoek JVD, Walters A, Devenish A (2018) Water stress and human migration: a global, geo-referenced review of empirical research. Food and Agriculture Organization of the United Nations. Rome. Water and Land discussion paper 11. ISBN 9251304262, 9789251304266
- Xie H, Longuevergne L, Ringler C, Scanlon BR (2012) Calibration and evaluation of a semi-distributed watershed model of Sub-Saharan Africa using GRACE data. *Hydrol Earth Syst Sci* 16:3083–3099. <https://doi.org/10.5194/hess-16-3083-2012>

Publisher's Note Springer Nature remains neutral with regard to jurisdictional claims in published maps and institutional affiliations.

Springer Nature or its licensor (e.g. a society or other partner) holds exclusive rights to this article under a publishing agreement with the author(s) or other rightsholder(s); author self-archiving of the accepted manuscript version of this article is solely governed by the terms of such publishing agreement and applicable law.

Authors and Affiliations

Amin Ibrahim¹ · Khaled S. Gemal^{2,5}  · Sayed Bedair³ · Saada A. Saada⁴ · Magaly Koch⁵ · Ahmed Nosair²

¹ Geology Department, Faculty of Science, Zagazig University, Zagazig 44519, Egypt

² Environmental Geophysics Lab (ZEGL), Faculty of Science, Geology Department, Zagazig University, Zagazig 44519, Egypt

³ The Research Institute for Groundwater (RIGW), Ministry of Water Resources and Irrigation, Kanater Khairia, Egypt

⁴ Geology Department, Faculty of Science, Suez University, Suez 43518, Egypt

⁵ Center for Remote Sensing, Earth and Environment Department, Boston University, Boston, MA 02215, USA